JOURNAL OF GEOPHYSICAL RESEARCH, VOL. 108, NO. C3, 3056, doi:10.1029/2001JC001240, 2003

Assimilation of drifter observations for the reconstruction of the Eulerian circulation field

Anne Molcard[1]
Rosenstiel School of Marine and Atmospheric Sciences, Division of Meteorology and Physical Oceanography (RSMAS/MPO), University of Miami, Miami, Florida, USA

Leonid I. Piterbarg
Center for Applied Mathematical Sciences, University of Southern California, Los Angeles, California, USA

Annalisa Griffa,[1] Tamay M. Özgökmen, and Arthur J. Mariano
Rosenstiel School of Marine and Atmospheric Sciences, Division of Meteorology and Physical Oceanography (RSMAS/MPO), University of Miami, Miami, Florida, USA

Received 3 December 2001; revised 19 July 2002; accepted 16 September 2002; published 1 March 2003.

[1] In light of the increasing number of drifting buoys in the ocean and recent advances in the realism of ocean general circulation models toward oceanic forecasting, the problem of assimilation of Lagrangian observations data in Eulerian models is investigated. A new and general rigorous approach is developed based on optimal interpolation (OI) methods, which takes into account directly the Lagrangian nature of the observations. An idealized version of this general formulation is tested in the framework of identical twin experiments using a reduced gravity, quasi-geostrophic model. An extensive study is conducted to quantify the effectiveness of Lagrangian data assimilation as a function of the number of drifters, the frequency of assimilation, and the uncertainties associated with the forcing functions driving the ocean model. The performance of the Lagrangian assimilation technique is also compared to that of conventional methods of assimilating drifters as moving current meters, and assimilation of Eulerian data, such as fixed-point velocities. Overall, the results are very favorable for the assimilation of Lagrangian observations to improve the Eulerian velocity field in ocean models. The results of our assimilation twin experiments imply an optimal sampling frequency for oceanic Lagrangian instruments in the range of 20–50% of the Lagrangian integral timescale of the flow field. *INDEX TERMS:* 4255 Oceanography: General: Numerical modeling; 4263 Oceanography: General: Ocean prediction; 3337 Meteorology and Atmospheric Dynamics: Numerical modeling and data assimilation; *KEYWORDS:* Lagrangian assimilation, drifters, Lagrangian velocity, Eulerian velocity, numerical model

Citation: Molcard, A., L. I. Piterbarg, A. Griffa, T. M. Özgökmen, and A. J. Mariano, Assimilation of drifter observations for the reconstruction of the Eulerian circulation field, *J. Geophys. Res.*, *108*(C3), 3056, doi:10.1029/2001JC001240, 2003.

1. Introduction

[2] In the last decade, deployment of drifting buoys has increased drastically and the data density is expected to increase in the coming years [*Mariano et al.*, 2002]. Lagrangian data are important for global ocean exploration because of their extensive horizontal coverage. Historically, they have been used primarily to compute statistical properties of the circulation, such as mean flow structure, second-order statistics, and transport properties [*Davis*, 1991; *Owens*, 1991; *Swenson and Niiler*, 1996; *Bauer et al.*, 1998; *Lavender et al.*, 2000; *Poulain*, 2001; *Fratantoni*, 2001; *Zhang et al.*, 2001]. Oceanic Lagrangian data stimulated development of novel methods to address issues of Lagrangian mixing and transport using tools based on dynamical system theory [*Wiggins*, 1992; *Poje and Haller*, 1999; *Coulliette and Wiggins*, 2000]. Lagrangian data are used in statistical modeling of particle motion [*Thomson*, 1986; *Griffa et al.*, 1995; *Griffa*, 1996; *Falco et al.*, 2000], for assimilating into Lagrangian stochastic models [*Özgökmen et al.*, 2000, 2001; *Castellari et al.*, 2001; *Piterbarg*, 2001] and for estimating Eulerian velocity fields [*Toner et al.*, 2001a, 2001b]. Presently, and even more so in the future, the increasing data density will allow their use not only in statistical studies, but also in prediction studies, for which they provide real-time measurements to complement numerical ocean circulation models. In particular, given recent advances in the realism of ocean general circulation models [*Smith et al.*, 2000; *Stammer and Chassignet*, 2000], assimilation of the information provided by Lagrangian instruments into ocean general circulation models for forecasting ocean velocity fields, is an important, timely, and challenging research problem.

[1] Also at Consiglio Nazionale Delle Ricerche, Istituto per lo Studio della Oceanografia Fisica (IOF), La Spezia, Italy.

0148-0227/03/2001JC001240$09.00

[3] Lagrangian instruments are floating buoys designed to move with the current and to communicate their position at discrete intervals of time Δt. Here, the focus is on instruments that provide real-time information via satellite, because they are directly relevant to the nowcasting/forecasting problem. These include near-surface drifters, and profiling floats moving in the subsurface at a certain reference level and resurfacing every Δt to communicate. In addition to the position, Lagrangian instruments also provide other types of information depending on the specific type of instruments, such as temperature and salinity profiles. All these data can be used for assimilation in numerical models. In this study, we focus on the assimilation of float positions into a numerical model for improving nowcasts of the Eulerian velocity field.

[4] There is a number of open issues connected with the assimilation of float positions. A central problem common to all Lagrangian data is that there is a nonlinear relationship between the observed variables, the positions $\mathbf{r}$, and the model variables to be modified, the Eulerian velocities $\mathbf{u}$. This nonlinear functional, $\mathbf{r} = \mathbf{H}(\mathbf{u})$, directly enters in the assimilation scheme, introducing significant difficulties in the formulation. When the time interval Δt between successive position measurements is small with respect to the Lagrangian integral timescale T_L (typically on the order of 1–3 days for the ocean surface and 7–10 days for subsurface) [e.g., *Griffa*, 1996], this problem can be circumvented by approximating $\mathbf{u}$ as finite difference of successive positions, $\mathbf{u} \approx \Delta\mathbf{r}/\Delta t$ [*Ishikawa et al.*, 1996; *Hernandez et al.*, 1995]. This approach, to which we will refer as "pseudo-Lagrangian," corresponds to the use of Lagrangian instruments as "moving current meters." In many cases, Δt is a sizable fraction of T_L, and this approach is expected to be inaccurate. In those cases, the Lagrangian nature of data needs to be directly addressed.

[5] In this paper, the assimilation of drifter positions in ocean models to improve velocity information is addressed by introducing a new formulation and conducting a comprehensive study to determine its performance.

[6] The formulation is introduced in the framework of the optimal interpolation (OI) method, and it addresses the difficulty introduced by the nonlinear relationship $\mathbf{H}(\mathbf{u})$ taking directly into account the Lagrangian nature of the observations. The formulation is general and can in principle account for information about the extended float path. As a first step, though, a simplified algorithm is introduced where only two successive positions are considered at each given time. This simplified algorithm is extensively tested numerically. Conceptually, the position increments of the floats during each assimilation time interval Δt are forecasted using the model, and the model Eulerian velocity field is modified in order to minimize the difference between observed and forecasted positions. The algorithm is tested using the classical "twin experiment" approach, and double-gyre circulations from a quasi-geostrophic reduced gravity model. Synthetic surface drifters are released in the "control" ocean and their positions are assimilated in the "assimilation" ocean. The dependence of the difference between Eulerian circulations in control and assimilation oceans on the various parameters of the problem, e.g., the sampling interval Δt, the wind forcing driving the models, and the number and launch positions of the drifters, are investigated and the robustness of the results is studied. The performance of assimilating drifter positions is also compared to the conventional technique of assimilating the drifter data as moving current meters, and assimilation of stationary current meter data.

[7] A reduced gravity, instead of a multilayer approach is preferred in this study for simplicity because multiple layers do not only interact in a complex manner, but they also require implementation of specific assimilation techniques to project surface information with fluid depth [*Chin et al.*, 2002]. Also, the quasi-geostrophic formulation has only one prognostic variable, i.e., the potential vorticity. Hence, this model is considerably simpler than primitive equation models, for the purpose of exploring the feasibility of Lagrangian data assimilation in Eulerian models. In primitive equation models, in fact, assimilated velocities have to be consistent with the other dynamical variables, such as density, in order to properly modify the solution without introducing spurious noise. Multilayer and multivariate dynamics are outside the scope of this initial feasibility study, and will be topics of future investigation.

[8] The assimilation of drifter trajectories in an ocean general circulation model was also investigated by *Kamachi and O'Brien* [1995]. The primary differences of the present study and that by *Kamachi and O'Brien* [1995] are as follows. *Kamachi and O'Brien* [1995] use an adjoint method and a variational formalism with a cost function measuring the distance between the trajectories of the model simulated drifters and the observed drifters. Generally, adjoint methods require significant coding, computation time, and need to be adapted for individual ocean models. Here, we present a technique that is not only highly portable, but also computationally very efficient. Second, we demonstrate that the difference in effectiveness between pseudo-Lagrangian and fully Lagrangian assimilation is only a function of the assimilation period Δt scaled by Lagrangian decorrelation timescale T_L, and this difference is quantified. As experiments have been performed for a single Δt by *Kamachi and O'Brien* [1995], they do not isolate exactly when the Lagrangian assimilation is more effective than classical techniques, and when it is not necessary to try to incorporate Lagrangian considerations in assimilation schemes.

[9] The paper is organized as follows. The mathematical background and the Lagrangian assimilation formulation are introduced in section 2. The numerical model and the experimental setup are discussed in section 3. The results are presented and discussed in section 4. A summary is provided in section 5 together with some remarks for future studies.

2. General Formulation for Lagrangian Data Assimilation

[10] The data assimilation problem can be approached in many different ways [*Bennett*, 1992; *Ghil and Malanotte-Rizzoli*, 1991]. In particular, three main approaches can be recognized on the basis of the relative importance which an investigator assigns to a model and observations. If it is required that the assimilated field satisfies the model equations, exactly or approximately, one readily arrives at the control theory set up, which in turn leads to multiple forward and backward integrations of the original and

adjoint equations. The observations are used to "correct" the model parameters, initial and boundary conditions, etc. This approach is hard to apply to nonlinear systems and is computationally expensive. However, when these difficulties are overcome, the method is very efficient, e.g. the review and references therein by *Evensen et al.* [1998].

[11] The second approach is the Kalman filter method, in which the assimilated field is not required to be the global solution of the model equations anymore, but instead the equations are used as a physically reasonable interpolator between sequential observations. There are also some computational difficulties, which have been effectively attacked lately [*Cane et al.*, 1996; *Chin et al.*, 1999]. As for the Lagrangian data assimilation, the Kalman filter was used by *Carter* [1989] for assimilating "RAFOS" floats in a simple shallow water model of the Gulf Stream.

[12] Finally, if the model and observations are treated as partners with equal rights, then the problem is to find a best (linear) combinations of them as the true field representation. Analytically and computationally, this is the simplest assimilation method, so we choose it for the present work. The Lagrangian data assimilation problem is a difficult one and it is quite reasonable to start with a simple method to establish a benchmark for implementing more sophisticated approaches.

[13] A theoretical basis for an OI of model output and observations is the following relationship based on general Bayesian theory [e.g., *Lorenc*, 2000]:

$$\mathbf{u}^a = \mathbf{u}^b + \mathbf{R}^b\mathbf{G}^T\left(\mathbf{G}\mathbf{R}^b\mathbf{G}^T + \mathbf{R}^o\right)^{-1}\left(\mathbf{y} - \mathbf{H}\left(\mathbf{u}^b\right)\right) \qquad (1)$$

where $\mathbf{u}^a$ is the model velocity vector after assimilation, $\mathbf{u}^b$ is the model velocity vector before assimilation, $\mathbf{y}$ is the vector of observations, $\mathbf{H}(\mathbf{u}^b)$ is the functional that relates model state variables to the observations, $\mathbf{R}^o$ is the observation error covariance matrix, $\mathbf{R}^b$ is the covariance matrix of the model uncertainty, superscript T stands for transposition, and, finally

$$\mathbf{G} = \frac{\delta\mathbf{H}\left(\mathbf{u}^b\right)}{\delta\mathbf{u}^b} \qquad (2)$$

is the derivative of the model-to-observation functional (sensitivity matrix). We interpret "vectors" $\mathbf{u}^a$ and $\mathbf{u}^b$ as assimilated and model Eulerian vector fields on a given grid during run time T_{ob}, respectively, and $\mathbf{y}$ as observed position increments computed from a set of particle trajectories observed during the same time T_{ob}.

[14] Equation (1) is optimal under the following conditions:

1. The prior distribution of the true velocity vector $\mathbf{u}$ is Gaussian with mean $\mathbf{u}^b$ and covariance $\mathbf{R}^b$. Thus, we suppose that a model gives an unbiased estimate of the real velocity field with Gaussian error characterized by $\mathbf{R}^b$.
2. The distribution of the observation vector $\mathbf{y}$ is Gaussian with mean $\mathbf{H}(\mathbf{u})$ and covariance $\mathbf{R}^o$. Hence, it is supposed that the observations are also unbiased and their error is characterized by $\mathbf{R}^o$. This error is determined by instrument accuracy and resolution.
3. The functional $\mathbf{H}(\mathbf{u})$ is linear, which implies that $\mathbf{G}$ is constant.

[15] In the discussed problem, the conjecture (listed in third condition above) is not true in general, even though it might approximately hold locally. Thus, in the considered case, (1) is not optimal. Nevertheless, we choose to pursue (1), because in nonlinear stochastic problems the optimal solution is almost never available and the hope is that the solution optimal in the linear case would perform in an acceptable way also in the nonlinear case. There is a full analogy between (1) and formulas for the extended Kalman filter (EKF) [*Carter*, 1989]. Although the EKF is not the optimal nonlinear filtering method, it is widely used in assimilation applications.

2.1. Assimilation Algorithm

[16] Consider M Lagrangian particles released at the same time $t = 0$ from different positions $\mathbf{r}_1^0, \mathbf{r}_2^0, \ldots, \mathbf{r}_M^0$ on the plane or isopycnic surface. Their motion is covered by the following system of $2M$ equations:

$$\frac{d\mathbf{r}_m}{dt} = \mathbf{u}(t, \mathbf{r}_m), \quad \mathbf{r}_m(0) = \mathbf{r}_m^0, \quad m = 1, \ldots, M,$$

where $\mathbf{u}(t, \mathbf{r})$ is a Eulerian velocity field, and $\mathbf{v}_m(t) = d\mathbf{r}_m/dt$ is the horizontal Lagrangian velocity of the m-th particle. Assume that the trajectories are observed with some errors in discrete moments $n\Delta t$, $n = 1, 2, \ldots, N$ and denote observations by $\mathbf{r}_m^o(n)$, while the corresponding quantities obtained from the model for the same initial conditions are denoted by $\mathbf{r}_m^b(n)$.

[17] Introduce finite difference Lagrangian velocity obtained from the position increments for observations and model, respectively

$$\mathbf{v}_m^o(n) = \frac{\Delta\mathbf{r}_m^o}{\Delta t} = \frac{\mathbf{r}_m^o(n) - \mathbf{r}_m^o(n-1)}{\Delta t},$$
$$\mathbf{v}_m^b(n) = \frac{\Delta\mathbf{r}_m^b}{\Delta t} = \frac{\mathbf{r}_m^b(n) - \mathbf{r}_m^b(n-1)}{\Delta t}$$

and let $\mathbf{u}_{ij}(n) = \mathbf{u}(n\Delta t, ih, jh)$ be the Eulerian velocity values on a grid with step h at moment n. Let

$$\epsilon = \Delta t \parallel \frac{D\mathbf{u}}{D\mathbf{r}} \parallel, \qquad (3)$$

where $D\mathbf{u}/D\mathbf{r}$ is the matrix of velocity spatial gradients and $\|\cdot\|$ is a matrix norm. Assume

$$\epsilon \ll 1. \qquad (4)$$

Condition (4) is true if the frequency of measurements is high enough to resolve the spatial gradients of the current. In this study, we mostly consider and evaluate the simplest assimilation formula. This formula can be obtained from the general relations (1) and (2) accounting for only zeroth-order terms in ϵ. The description of a possible generalization of this formula is given in section 2.3, where the assimilation formula (15) accounts for the first-order terms in ϵ. A detailed derivation of (5) and (15) from (1) and (2) is given in Appendix A.

[18] The zeroth-order simplest assimilation formula is

$$u_{ij}^a(n) = u_{ij}^b(n) + \alpha^{-1}\sum_{m=1}^{M}\gamma_{ijm}\left(u_m^o(n) - u_m^b(n)\right),$$
$$v_{ij}^a(n) = v_{ij}^b(n) + \alpha^{-1}\sum_{m=1}^{M}\gamma_{ijm}\left(v_m^o(n) - v_m^b(n)\right), \qquad (5)$$

The velocity components u, v with subs (ij) are Eulerian velocities at the corresponding grid point, while the same variables u, v supplied with the single sub (m) stand for the Lagrangian velocity components of the m-th drifter. Here

$$\gamma_{ijm} = E_h\left(x_m^b(n) - ih, y_m^b(n) - jh\right), \quad E_h(x,y) \equiv \exp\left(-\frac{x^2}{2h^2} - \frac{y^2}{2h^2}\right) \tag{6}$$

and

$$\alpha = 1 + \sigma_o^2/\sigma_b^2, \tag{7}$$

σ_b^2 is the modeling velocity mean square error and σ_o^2 is the error for the Lagrangian velocity which is related to the error of independent positions, say σ_r^2, by $\sigma_o^2 = \sigma_r^2/\Delta t^2$. When deriving (5), we also assume that the errors of both model and observed variables are uncorrelated in time and space, i.e., matrices $\mathbf{R}^b$ and $\mathbf{R}^o$ in (1) are diagonal. One of the important steps in this derivation is an expression for the variational derivative of the drifter position with respect to the Eulerian velocity. Coefficients gamma's in (5) come from approximating the delta function appearing in this derivative by the Gauss function.

[19] Notice that the simplified expression (5) takes into account only one assimilation time step Δt, or equivalently only two successive data points. Conceptually, then, it does not fully introduce the information on particle paths. Rather, it converts the position information into Lagrangian velocity information $\mathbf{v}$, i.e., velocity averaged along particle trajectories during the time Δt. $\mathbf{v}^b$ is computed in the model by generating trajectories during Δt and using the two end points. The simplified algorithm (5), which is the focus of the present paper, can be considered as a first step in the implementation of the general formulation (1) and (2). Possible generalizations to multistep algorithms, including more extended path informations, are discussed in Appendix A and in section 2.3, where an explicit formula for the two time step algorithm is given.

2.2. "Pseudo-Lagrangian" Assimilation

[20] Now we compare the assimilation formula (5) with "pseudo-Lagrangian" assimilation. The pseudo-Lagrangian formulation is simpler than the fully Lagrangian formulation, since it assumes that the observed and model variables are the same. In the pseudo-Lagrangian assimilation, trajectories and Lagrangian velocities are not computed using the model, but rather the model Eulerian velocity $\mathbf{u}^b$ is directly used. In the limit of small Δt, Lagrangian and Eulerian velocities indeed coincide, and therefore the pseudo-Lagrangian assimilation is expected to provide similar results with respect to the full Lagrangian assimilation. For finite Δt, though, the differences between the two methods are expected to be relevant. In the pseudo-Lagrangian assimilation, the functional $\mathbf{H}$ is linear and $\mathbf{G}$ is constant in the OI formulation. In other words, the difference between the observed Lagrangian velocity $\mathbf{v}^o$ and the Eulerian model velocity $\mathbf{u}^b$ appears directly in the correction term in (1).

[21] In the following, we compare the procedure (5) written in vector form

$$\mathbf{u}_{ij}^a(n) = \mathbf{u}_{ij}^b(n) + \alpha^{-1}\sum_{m=1}^{M}\gamma_{ijm}\left(\mathbf{v}_m^o(n) - \mathbf{v}_m^b(n)\right), \tag{8}$$

with the local pseudo-Lagrangian procedure,

$$\tilde{\mathbf{u}}_{ij}^a(n) = \mathbf{u}_{ij}^b(n) + \alpha^{-1}\sum_{m=1}^{M}\gamma_{ijm}\left(\mathbf{v}_m^o(n) - \mathbf{u}_m^b(n)\right). \tag{9}$$

where

$$\mathbf{u}_m^b(n) = \mathbf{u}^b(n\Delta t, \mathbf{r}_m(n\Delta t))$$

is the Eulerian velocity at the drifter position found by interpolating grid velocities. For the sake of simplicity assume that the observations are almost perfect ($\alpha \approx 1$), and that for a given grid point (i, j) only one observed trajectory is passing through this point, while other drifters are far enough from this grid point. The latter means

$$\mathbf{u}_m^b(n) = \mathbf{u}_{ij}^b(n),$$

where the subscript m is referred to the observed trajectory. Thus, (8) and (9) become

$$\mathbf{u}_{ij}^a(n) \approx \mathbf{u}_{ij}^b(n) + \mathbf{v}_{ij}^o(n) - \mathbf{v}_{ij}^b(n), \tag{10}$$

and

$$\tilde{\mathbf{u}}_{ij}^a(n) \approx \mathbf{v}_{ij}^o(n), \tag{11}$$

where $\mathbf{v}_{ij}^o(n)$ and $\mathbf{v}_{ij}^b(n)$ are observed (real) and modeled Lagrangian velocities respectively at the point (i, j) at moment n. The ratio r of the assimilation error for (10) and (11) becomes

$$r \equiv \frac{\left|\mathbf{u}_{ij}^a(n) - \mathbf{u}_{ij}^o(n)\right|}{\left|\tilde{\mathbf{u}}_{ij}^a(n) - \mathbf{u}_{ij}^o(n)\right|} = \frac{\left|\mathbf{u}_{ij}^b(n) - \mathbf{v}_{ij}^b(n) + \left(\mathbf{v}_{ij}^o(n) - \mathbf{u}_{ij}^o(n)\right)\right|}{\left|\mathbf{v}_{ij}^o(n) - \mathbf{u}_{ij}^o(n)\right|}. \tag{12}$$

By neglecting the Eulerian velocity time derivative one can obtain the following decomposition

$$\mathbf{v}_{ij}^{b,o}(n) \approx \mathbf{u}_{ij}^{b,o}(n) - \mathbf{D}_{ij}^{b,o}(n)\mathbf{u}_{ij}^{b,o}(n),$$

where

$$\mathbf{D}_{ij}(n) = \frac{\Delta t}{2}\begin{pmatrix} \partial u_{ij}(n)/\partial x & \partial u_{ij}(n)/\partial y \\ \partial v_{ij}(n)/\partial x & \partial v_{ij}(n)/\partial y \end{pmatrix}, \tag{13}$$

the ratio of the assimilation errors from fully Lagrangian and pseudo-Lagrangian methods becomes

$$r = \frac{\left|\mathbf{D}_{ij}^b(n)\mathbf{u}_{ij}^b(n) - \mathbf{D}_{ij}^o(n)\mathbf{u}_{ij}^o(n)\right|}{\left|\mathbf{D}_{ij}^o(n)\mathbf{u}_{ij}^o(n)\right|}. \tag{14}$$

This quantity will be used in the comparison of fully Lagrangian and pseudo-Lagrangian assimilation schemes presented in section 4.6.

2.3. Extensions of the Assimilation Algorithm

[22] The goal of this paper is a comprehensive investigation of the simplest assimilation algorithm (5). This algorithm is local, in both time and space, in the sense that it uses only the observations made at the same time moment and the

nearest observations in space. Locality in time comes from neglecting terms of order ε in (1) and (2) or, equivalently, the matrix **G** is replaced by a diagonal matrix with the same diagonal elements. Locality in space is due to the assumption of diagonality of the covariance matrices involved in (1). Thus, more sophisticated and potentially more powerful assimilation procedures can be obtained by accounting for the terms of higher order in ε and incorporating spatial correlations to the model and/or observation errors. In particular, still assuming uncorrelated errors, but replacing **G** in (1) and (2) by a two-diagonal matrix, we get the following two-step assimilation algorithm (see Appendix A)

$$\begin{aligned} u^a_{ij}(n) = u^b_{ij}(n) + \sum\nolimits_{m=1}^{M} \Big\{ \gamma_{ijm} \Big(\alpha^{-1} \big(u^o_m(n) - u^b_m(n) \big) \\ - 2\alpha^{-2} \Big(d^{11}_{ij}(n) \big(u^o_m(n-1) - u^b_m(n-1) \big) \\ + d^{12}_{ij}(n) \big(v^o_m(n-1) - v^b_m(n-1) \big) \Big) \Big) \Big\}, \\ v^a_{ij}(n) = v^b_{ij}(n) + \sum\nolimits_{m=1}^{M} \Big\{ \gamma_{ijm} \Big(\alpha^{-1} \big(v^o_m(n) - v^b_m(n) \big) \\ - 2\alpha^{-2} \Big(d^{21}_{ij}(n) \big(u^o_m(n-1) - u^b_m(n-1) \big) \\ + d^{22}_{ij}(n) \big(v^o_m(n-1) - v^b_m(n-1) \big) \Big) \Big) \Big\}, \end{aligned} \tag{15}$$

where terms of order $O(\alpha - 1)$ are omitted and

$$\begin{pmatrix} d^{11}(n) & d^{12}(n) \\ d^{21}(n) & d^{22}(n) \end{pmatrix} = \mathbf{D}_m(n)$$

is essentially the same gradient matrix as in (13), but taken at the position of m-th drifter at the moment n. This procedure involves trajectories observations at the moments $n-2, n-1, n$ as well as the model velocity gradients along the observed trajectories.

[23] In general, there is no essential analytical difficulties in constructing multistep assimilation procedures since we have developed a general assimilation formula (A19) with all the quantities well defined and the general expression (A14) for the entries of the most important matrix **G**. Another class of assimilation procedures can be obtained by introducing space correlations to the modeled error. If the introduced correlation scale is d, then the corresponding algorithm involves observations within radius d of the assimilation point. Explicit procedures can be developed on the base of expressions for entries of the matrices involved in (1) (see (A3), (A4), and (A7) in Appendix A). Detailed derivation and investigation of nonlocal interpolation procedures is beyond the scope of this paper and will be a subject of further research.

3. The Numerical Model and Experimental Setup

[24] The quasi-geostrophic reduced gravity model equations are:

$$\frac{\partial q}{\partial t} + J(\psi, q) = \frac{f_0}{H} w_E + \nu \nabla^4 \psi - r \nabla^2 \psi, \tag{16}$$

Table 1. Parameters of the Reduced Gravity Quasi-Geostrophic Model

Basin size (x,y)	2000×2000 km^2
Coriolis parameters	$f_0 = 7.3 \times 10^{-5}$ s^{-1}, $\beta = 2 \times 10^{-11}$ m^{-1} s^{-1}
Layer thickness	$H = 1000$ m
Reduced gravity	$g' = 0.01$ m s^{-2}
Deformation radius	$R_d = 42$ km
Eddy viscosity	$\nu = 200$ m^2 s^{-1}
Horizontal grid scale	$\Delta x = \Delta y = 20$ km
Interfacial friction coefficient	$r = 5 \times 10^{-8}$ s^{-1}
Time step	1.6 hours

where q is the potential vorticity defined by

$$q = \nabla^2 \psi + \beta y - \frac{1}{R_d^2} \psi. \tag{17}$$

Here, ψ is the geostrophic stream function, f_0 is the Coriolis frequency at a reference latitude, β is the meridional gradient of the Coriolis frequency, $R_d = \sqrt{g'H}/f_0$ is the radius of deformation, g' is the reduced gravity, H is the active layer depth, w_E is the Ekman velocity field proportional to the wind stress curl, ν is the horizontal eddy viscosity, r is the interfacial friction coefficient and $\nabla^2 = \frac{\partial^2}{\partial x^2} + \frac{\partial^2}{\partial y^2}$ is the horizontal Laplacian operator.

[25] A nondimensionalized form of the prognostic equation (16) is advanced in time using a predictor-corrector type of leapfrog method [*Gazdag*, 1976]. The Jacobian operator $J(\psi, q) = \frac{\partial \psi}{\partial x}\frac{\partial q}{\partial y} - \frac{\partial q}{\partial x}\frac{\partial \psi}{\partial y}$ is computed using the formulation proposed by *Arakawa* [1966] that conserves kinetic energy and enstrophy, and satisfies the antisymmetry property $J(\psi, q) = -J(q, \psi)$. The diagnostic equation (17) is inverted using a Gauss–Seidel iteration technique.

[26] The model is configured in a square domain of 2000×2000 km^2 and centered at 30°N. The equilibrium layer thickness is taken as 1000 m, and the stratification is such that the Rossby radius of deformation is approximately 42 km, typical of midlatitude circulation. An idealized double-gyre configuration is adopted for the experiments, since this is probably the best-known setup in ocean modeling since the study by *Holland* [1978] and the dynamics of which, Sverdrup gyres, western boundary currents, midlatitude jet and mesoscale eddies, are familiar to oceanographers. The wind forcing, sinusoidally varying with latitude, drives subtropical and subpolar gyres of equivalent strength of 30 Sv along the western boundary. The eddy viscosity coefficient is taken as $\nu = 200$ m^2 s^{-1} such that the viscous boundary layer scale $(\nu/\beta)^{1/3}$ is larger than the grid spacing of 20 km. No normal flow and free-slip conditions are applied along all boundaries. The parameters of the numerical model are summarized in Table 1.

3.1. Identical Twin Experiments and Assimilation Implementation

[27] In order to exactly quantify the performance of the data assimilation scheme, the identical twin experiment approach is used (Figure 1). First, the model is integrated for 20 years until the Rossby waves cross the basin, enhance the western boundary current and the midlatitude jet, and the model energetics reach a statistically steady state. Synthetic surface drifters are then launched in the model and advected with the model velocity field using a fourth-order Runge–Kutta scheme with the same time step of 1.6 hours used for the model integration. Therefore, the exact

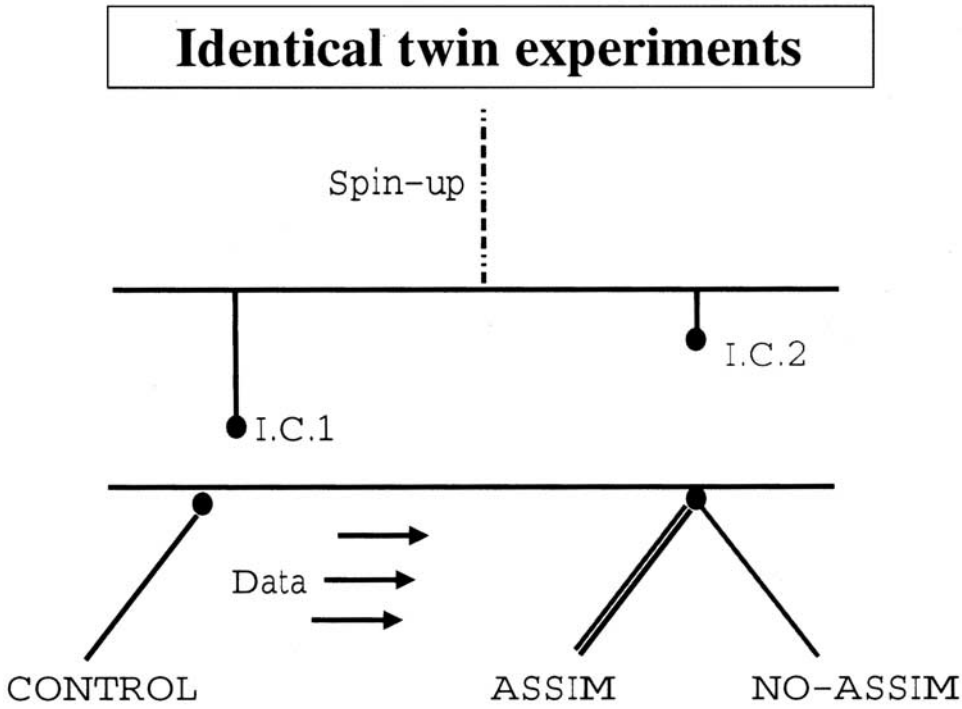

Figure 1. Schematic depiction of identical twin experiments.

Eulerian velocity field, or the so-called ''control'', generating the ''observed data'' or positions of drifters, is known in this approach.

[28] The drifter data are then assimilated into another model run, the so-called ''assimilation'' run, which has one of these two characteristics: (1) has the same parameters as the control case but starts from a different initial conditions during the statistically steady state, which simulates the effect of not knowing the exact state of the ocean in reality, or (2) is subject to a different wind stress forcing, which allows us to explore the impact of not knowing the exact forcing functions acting on the ocean. A third experiment, the so-called ''no-assimilation'' run, depicts the state of the model evolution without assimilation of drifter data.

[29] In all the experiments, the assimilation of the drifter positions is performed using the algorithm (5). We recall that this algorithm is obtained under the following assumptions: (1) the model error is spatially uncorrelated and (2) the sensitivity matrix **G** equation (2) is approximated using a linear, zeroth-order expansion of **r**(**u**), so that the velocity gradient does not enter in **G**. It is worth mentioning that in equation (5), a certain degree of smoothing is maintained, even in absence of error structure, by the Gaussian function approximation to the delta function in **G**(A8). Also, it can be expected that for the quasi-geostrophic equation, smoothing is provided by the elliptic equation (17), so that the error correlation function is expected to play a somewhat less important role than in the case of assimilation in primitive equation models.

[30] From the practical point of view, the assimilation (5) is implemented in the following way (Figure 2). Let us assume that a drifter position $\mathbf{r}^o(t_0)$ is observed at time t_0(A). The model is forwarded in time from t_0 to $t_0 + \Delta t$, providing a forecast of the drifter path starting from $\mathbf{r}^o(t_0)$. The forecasted drifter will reach a certain position $\mathbf{r}^b(t_0 + \Delta t)$, (C), and it will be characterized by a position increment $\Delta\mathbf{r}^b$ and a Lagrangian velocity $\mathbf{v}^b = \Delta\mathbf{r}^b/\Delta t$. The forecasted $\mathbf{v}^b$ is then compared with the observed Lagrangian velocity $\mathbf{v}^o$ at $t_0 + \Delta t$. The model Eulerian velocity $\mathbf{u}^b(t_0)$ is modified in the vicinity of $\mathbf{r}^o(t_0)$, as a function of the difference between forecast (C) and observation (B) using (5). From the modified $\mathbf{u}^a(t_0)$ field, first the modified relative vorticity, and then $\psi(t_0)$ is computed inverting the finite difference matrix representation of (17). The model is then advanced forward again, starting from t_0 to $t_0 + \Delta t$, using the modified ψ. The parameter α defined in (7) has been chosen on the basis of the ratio σ_r^2/σ_b^2, which is varied between 10^4 and 10^8 s^2. This corresponds to a regime in which the Lagrangian position error σ_r is on the order of 10–100 m and modeling velocity error σ_b is on the order of 1–10 cm s^{-1}. Those values give for α defined as $\alpha = 1 + \frac{1}{\Delta t^2}\frac{\sigma_r^2}{\sigma_b^2}$ a range of values going from 1.01 for small sampling period to 1.001 for higher Δt.

[31] The success of the assimilation in the experiments is evaluated both qualitatively and quantitatively. Qualitatively, the stream function patterns of the control, assimilation and no assimilation runs are visually compared at different times. Quantitatively, two different overall measurements of the difference between control and assimilation have been considered and evaluated during the experiment time evolutions:

$$Eru = \frac{\sqrt{\left(\sum (u_c - u_a)^2 + (v_c - v_a)^2\right)/K}}{\sqrt{\left(\sum (u_c^2 + v_c^2)\right)/K}} \quad \text{and} \quad Er\psi = \frac{\sqrt{\left(\sum (\psi_c - \psi_a)^2\right)/K}}{\sqrt{\left(\sum \psi_c^2\right)/K}}, \tag{18}$$

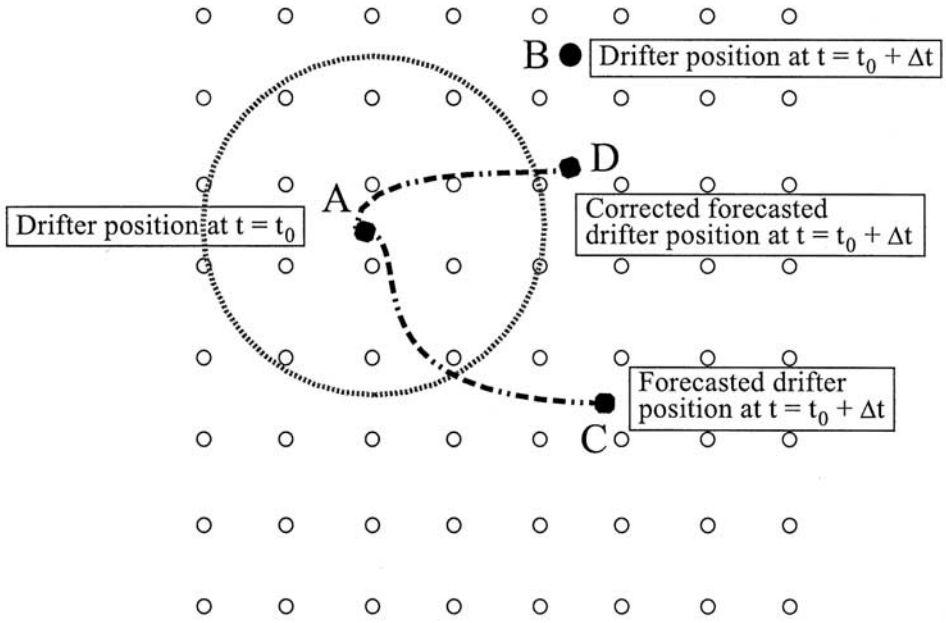

Figure 2. Schematic illustration of the assimilation algorithm. Given the drifter positions at $t = t_0$ (A) and $t = t_0 + \Delta t$ (B), the model forecast at $t = t_0 + \Delta t$ is improved from (C) to (D) by modifying the model Eulerian circulation field at $t = t_0$ within a circle of influence (model grid layout is shown in the background) using algorithm (5), which acts to minimize the distance between positions (B) and (C). The drifter position data are given at discrete time interval Δt, whereas the model simulated drifters can follow paths as shown between forecasted and corrected positions, (AC) and (AD), respectively.

where *Eru* and *Er*ψ define the RMS of the velocity and stream function difference between control ("c") and assimilation ("a") runs normalized by the corresponding RMS values of the control. Note that *Eru* is a stricter measure than *Er*ψ because it is based on the velocity that corresponds to the gradient of the stream function. In the following, only the behavior of *Eru* is shown for simplicity. The behavior of *Er*ψ is qualitatively similar, and the values are typically smaller, approximately by a factor of 1.6.

4. Results

[32] In this section, a series of experiments is presented, following the approach described above and aimed at quantifying the efficiency of the Lagrangian assimilation method. A base experiment, EXP-BASE, which will be used as a benchmark, is presented first and described in detail. The robustness of the results of EXP-BASE is then tested by varying the parameters of the problem: the sampling period Δt, the wind forcing, the number and the initial positions of the drifters. These parameters are changed in a realistic range in order to provide guidance for applications in the real ocean.

[33] A quantitative comparison between the performance of the full Lagrangian formulation (5) with respect to the "pseudo-Lagrangian" scheme (9), which approximates the Lagrangian velocity $\Delta \mathbf{r}/\Delta t$ using the Eulerian velocity at the drifter position is carried out. Finally, a comparison between assimilation of Lagrangian data and assimilation of Eulerian data, such as those provided by current meters, is presented.

4.1. The Base Experiment

[34] The basic characteristics of the benchmark experiment, EXP-BASE, are summarized in Table 2. A cluster of 25 drifters are released in the energetic western central region corresponding to the meandering jet and to the recirculations, in a box of 600 × 600 km (see Figure 3a). A set of 25 drifters has been chosen in order to have a number of Lagrangian data comparable to the number realistically available in the real ocean. WOCE/ARGO planned density is of the order of 1 float per 5° × 5°, hence roughly in the neighborhood of 20 floats total over our domain of 2000 × 2000 km^2. Also, we anticipate that, as shown in section 4.4, the assimilation results do not change drastically for higher data density up to 200 drifters. The control solution is nonlinear and nonstationary, with the RMS velocity of the order of 10 cm s^{-1} and the surface Lagrangian timescale of the order of $T_L \approx 10$ days (estimated as *e*-folding timescale). With respect to the real ocean, the model is characterized by longer timescales, similar to the Lagrangian timescales of the subsurface ocean. This is not surprising, given the simplified dynamics and the steady forcing [*Garraffo et al.*, 2001; *Berloff and McWilliams*, 2002].

[35] The initial conditions for the assimilation and no assimilation runs are identical (Figures 3c and 3d), but different from that for the control run (Figure 3b) as described in the identical twin experiment setup (Figure 1). All model parameters are identical in the control, assimilation and no assimilation runs.

[36] At $t > 0$, the assimilation of the drifter positions starts, with a sampling period $\Delta t = 1.6$ hours, which corresponds to the time step of the model, so that the assimilation is performed at each model time step. We anticipate that the results are also very similar for longer Δt, approximately up to 2 days, as discussed in detail in section 4.2. The spaghetti diagrams of the drifters are shown

Table 2. Characteristics and Parameters of the Experiments

Experiment	Assimilation Type	Assimilation Forcing	Measurement Type	Measurement Location	Δt
EXP-BASE	Lagrangian	control	25 drifters	central western region	1.6 hours–20 days
EXP-FORCE1	Lagrangian	1.5 × control	25 drifters	central western region	2 days
EXP-FORCE2	Lagrangian	0.5 × control	25 drifters	central western region	2 days
EXP-DRIFT-9–196	Lagrangian	control	9–196 drifters	central western region	2 days
EXP-DRIFT-25 a–h	Lagrangian	control	25 drifters	various locations	2 days
EXP-PSEUDO	pseudo Lagrangian	control	25 drifters	central western region	1.6 hours–20 days
EXP-EUL-25	Eulerian	control	25 current meters	central western region	1.6 hours–3 days
EXP-EUL-9	Eulerian	control	9 current meters	central western region	1.6 hours–3 days

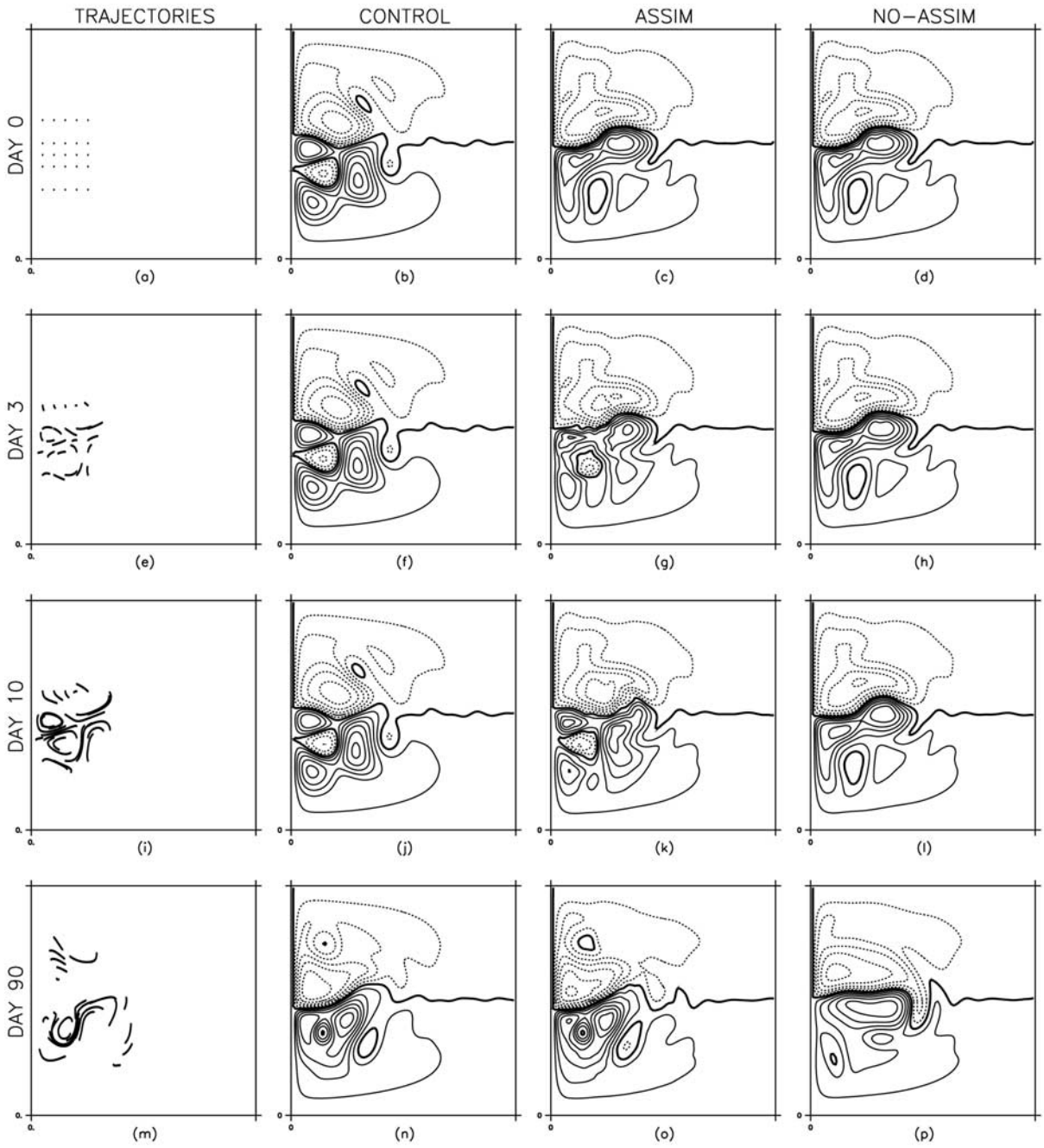

Figure 3. Drifter trajectories (a, e, i, and m), transport stream function (contour interval: 10 Sv) for the control (b, f, j, and n), assimilation (c, g, k, and o), and no-assimilation (d, h, l, and p) oceans at selected times (t = 0, 3, 10, and 90 days) for EXP-BASE. Spaghetti diagram (m) is shown from t = 70 days to t = 90 days. Note the rapid transition of the assimilation ocean circulation from the no-assimilation case to the control case.

Table 3. Summary of *Eru* of the Experiments

Experiment	Δt	Eru (%)
EXP-BASE	1.6 hours–20 days	18–87
EXP-FORCE1	2 days	65
EXP-FORCE2	2 days	29
EXP-DRIFT-9–196	2 days	58–11
EXP-DRIFT-25 a–h	2 days	22–110
EXP-PSEUDO	2 days	27–92
EXP-EUL-25	2 days	41
EXP-EUL-9	2 days	67

in Figures 3a, 3e, 3i, and 3m (trajectories are shown from t = 70 days to t = 90 days). During the simulation, most of the drifters remain in the western central region, trapped in the main circulation gyres. The transport stream functions demonstrate that the assimilation of drifter positions is highly effective after 10 days, leading to a quick convergence of the assimilation toward the control (Figures 3b–3d and 3j–3l). This first phase is followed by a slower but continuous convergence. After the first few months, some of the drifters might leave the highly energetic region, and reduce the efficiency of the assimilation. As a compromise, we choose to stop the simulation at t = 90 days. The patterns of control and assimilation runs are nearly identical at t = 90 days (Figures 3n and 3o), while the no assimilation run appears completely different (Figure 3p). The error between control and assimilation runs at t = 90 days is *Eru* $\approx$ 20% (Table 3). Overall, the results are highly satisfactory.

[37] In order to investigate that the rapid transition of assimilation run from no assimilation to control flow is independent of the specific realization, three other experiments have been performed starting from different initial flow patterns. The results are similar to that described above, with a difference of at most 10% in *Eru*. Therefore, the generality of the EXP-BASE results is confirmed.

4.2. Sensitivity to the Sampling Period Δt

[38] In the real ocean, the sampling period of the Lagrangian instruments can vary widely, typically ranging from a few minutes to a few days for drifters in the upper ocean, and from 8 hours to 1–2 weeks for SOFAR, RAFOS and profiling floats in the subsurface. Given the wide range of Δt, it is important to understand the sensitivity of the results to its changes.

[39] A series of experiments has been performed maintaining the same configuration as in EXP-BASE, but changing the value of the sampling period Δt (Table 2). The convergence characteristics are shown in Figure 4a, in

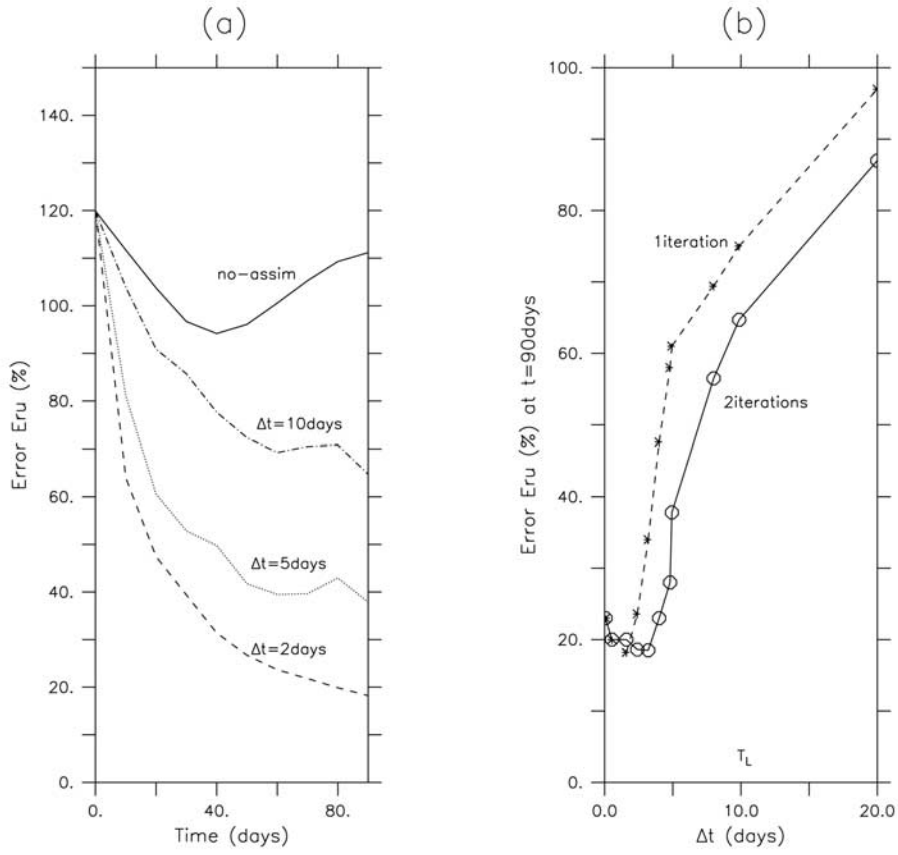

Figure 4. (a) Convergence error *Eru* (%) as a function of observation time in EXP-BASE using different sampling periods Δt = 2, 5, and 10 days in assimilation runs (dashed lines) and that of the no-assimilation case (solid line). (b) Error *Eru* at t = 90 days at a function of sampling period Δt for a single iteration (dashed line with "*") and two iterations (solid line with "o") per assimilation cycle. Lagrangian timescale is T_L = 10 days.

which *Eru* is plotted for 90 days for experiments with Δt = 2, 5, and 10 days (dashed lines). For comparison, *Eru* corresponding to the no assimilation experiment is also displayed (solid line), which shows that the normalized RMS error between the no assimilation and the control cases maintains values between 95% and 120% during the observation period of 90 days. In contrast, *Eru* in all assimilation runs decreases very quickly in the first 10 days, and then it keeps decreasing at a slower rate. The best results are obtained using Δt = 2 days, and the convergence characteristics deteriorate gradually for longer sampling periods.

[40] A summary of the results for 1.6 hours $\leq \Delta t \leq$ 20 days is provided in Figure 4b, where the values of *Eru* computed at t = 90 days are plotted (dashed line with "*"). For reference, the value of $T_L \approx$ 10 days is marked. As it can be seen, *Eru* remains low for Δt in the range between 1.6 hours and 2 days, with values of less than 24%. At closer inspection a minimum can be observed, corresponding to $\Delta t \approx$ 2 days. This minimum, even though not very pronounced, appears to be significant since it is present also in the simulations performed with different initial conditions. The reasons for its occurrence will be discussed in the following. For $\Delta t >$ 2 days, the error starts to increase, reaching values of *Eru* $\approx$ 61% for Δt = 5 days, *Eru* $\approx$ 75% for Δt = 10 days and *Eru* $\approx$ 97% for Δt = 20 days.

[41] The error for $\Delta t >$ 2 days can be reduced by repeating the assimilation procedure (Figure 2) for each time interval Δt more than once, using (5) to minimize the distance between points (C) and (B), and then (D) and (B), and so on. A priori indication that such an iterative process can be effective is given by the theoretical error estimate for the one-step procedure derived in section 2.3,

$$Er = \| \mathbf{u}^a - \mathbf{u}^o \| \approx \| \mathbf{D}^b \mathbf{u}^b - \mathbf{D}^o \mathbf{u}^o \|, \qquad (19)$$

where **D** is given by (13). As it can be seen, the error (19) can converge to zero for finite Δt provided that the model velocity gradient is sufficiently similar to the truth gradient. The convergence of the model to the truth can be accelerated by iterating the process.

[42] This iterative procedure has been tested in a number of experiments, and it has been proven to be effective for $\Delta t >$ 2 days. The results obtained with two iterations appear to be optimal in most cases, and they are shown in Figure 4b (solid line with "o"). The error *Eru* for Δt = 5 days is reduced from 61% to 38%, and at Δt = 10 days from 75% to 65%. For Δt = 20 days, despite the reduction, the error value remains high ($\approx$87%). This can be expected given that the content of information on the velocity is highly degraded for $\Delta t > T_L$. The other noticeable feature of Figure 4b is the evident delay between the two lines. The optimal sampling period is increased from 2 days with one iteration to 3 days with two iterations, and the optimal range (to obtain an error less than 20%) is enlarged from $\Delta t <$ 2 to $\Delta t <$ 3 days. In the following, for $\Delta t >$ 2 days, we will always refer to results obtained with 2 iterations of assimilation.

[43] The presence of the minimum error in Figure 4b can be explained, at least qualitatively, in the following way. The assimilation procedure introduces a small numerical error, related to the computation of the flow field ψ from the corrected velocity $\mathbf{u}^a$. The size of the numerical error has been evaluated in a series of preliminary runs where control and assimilation were started from the same initial condition. In these experiments, the assimilation runs appear to diverge slightly from the control. The assimilation error after 10 days is *Eru* $\approx$ 10% for Δt = 1.6 hours, whereas *Eru* $\approx$ 0.8% for Δt = 2 days, due to the fact that the assimilation is performed more frequently for Δt = 1.6 hours. The phase mismatch between the data from control run and the fields from the simulation with assimilation leads to constant injection of high frequency noise that is amplified by the nonlinear flow. We believe that this same mechanism is also responsible for the observed minimum in the present experiments.

[44] In order to gain more insight on the results, the behavior of *Eru* as function of time and the patterns of the solutions at t = 90 days are considered (Figures 4 and 5). Three selected solutions are shown, obtained using Δt = 2, 5, and 10 days. As it can be seen, the solution pattern for Δt = 2 days (Figure 5b), corresponding to the minimum error (*Eru* $\approx$ 18%) in Figure 4b, is nearly identical to the control (Figure 5a). For Δt = 5 days (Figure 5c), the pattern is still quite similar to the control and the error maintains relatively low (*Eru* $\approx$ 38%). For Δt = 10 days (Figure 5d), the error is higher (*Eru* $\approx$ 65%), but there is still a clear improvement with respect to the no-assimilation (Figure 3p), with the solution resembling the average between control and no-assimilation. This is an indication that the global error *Eru* is a quite strict measure of the assimilation results.

[45] The present results can be used to suggest recommended values for Δt in the ocean, using appropriate scaling by T_L. In the model, optimal performances are obtained for $\Delta t \approx T_L/5$. For the ocean surface, with $T_L \approx$ 1–3 days, this implies $\Delta t \approx$ 5–15 hours, while for the subsurface with $T_L \approx$ 7–10 days, $\Delta t \approx$ 1.5–2 days. For higher Δt, the error is still limited and the solution is still close to the control up to $\Delta t \approx T_L/2$, i.e., $\approx$0.5–1.5 days for the surface and $\approx$3.5–5 days for the subsurface.

4.3. Sensitivity to Model Forcing

[46] With the objective of exploring the efficiency of the assimilation technique in the case when the knowledge of forcing driving oceanic circulation (in addition to the knowledge of the initial conditions) is poor, an experiment denoted EXP-FORCE1 has been performed (Table 2). In this experiment, 20 years of spin-up is conducted using a wind forcing having the same structure as that in EXP-BASE, but an amplitude 50% higher such that Sverdrup gyres attain a transport of 45 Sv along the western boundary. The assimilation and no-assimilation runs have then been initialized using this spin-up, and this high wind forcing is maintained throughout the observation period, whereas the wind forcing acting on the control ocean is kept the same as in EXP-BASE (generating gyres with strengths of 30 Sv). The same drifter trajectories are considered as before (Figures 3a, 3e, 3i, and 3m) and their positions are assimilated using Δt = 2 days. Since the difference in the wind forcing between assimilation and control runs is quite substantial, we expect that the results will provide an extremely challenging test for the effective-

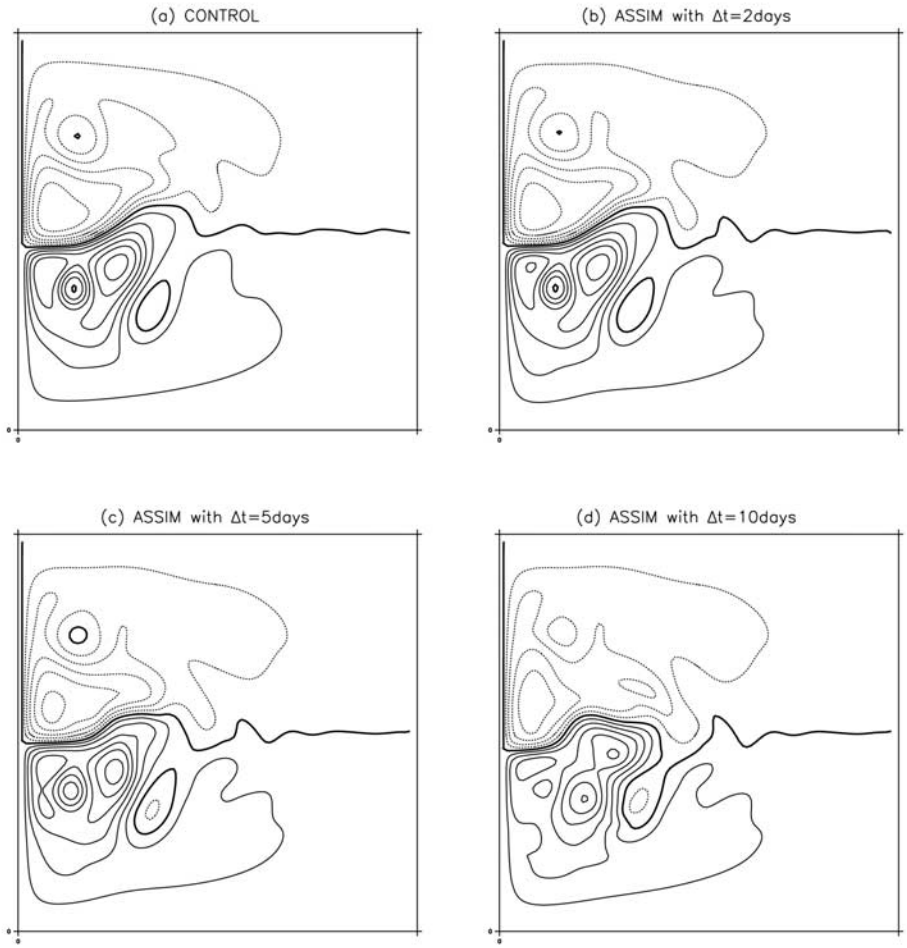

Figure 5. Transport stream function (ci: 10 Sv) at t = 90 days for (a) control run, (b) assimilation run using Δt = 2 days (*Eru* $\approx$ 18%), (c) assimilation run using Δt = 5 days (*Eru* $\approx$ 38%), and (d) assimilation run using Δt = 10 days (*Eru* $\approx$ 65%) in EXP-BASE.

ness of the assimilation algorithm. An observation period of 180 days is considered anticipating a slower convergence in this experiment.

[47] Snapshots of the solutions for control, assimilation and no-assimilation runs at t = 90 and 180 days are shown in Figure 6. The patterns of the assimilation run indicate a clear convergence toward the control. At t = 90 days, the assimilation solution (Figure 6b) looks like an average between control and no assimilation (Figures 6a and 6c), while at t = 180 days the resemblance to the control is much more clear (Figures 6d and 6e). In regions where there is drifter information, the assimilation run has lost all its memory, while in the other regions the pattern is still similar to the no-assimilation run. The corresponding *Eru* values are 72% and 65% at t = 90 days and t = 180 days, respectively. These values appear high, but as demonstrated above, *Eru* is a quite strict measure of error. Also, it should be noted that this experimental run is characterized by a considerably higher energy, due to the higher forcing maintained throughout the simulation. The slow convergence is expected given that in this case the wind works "against" the assimilation, i.e., it tends to drive the assimilation run away from the control.

[48] In the previous experiment, the assimilation of drifter data is able to reduce significantly the energy level despite the high wind forcing, therefore acting as a dissipative mechanism. For assimilation of real drifter data in ocean circulation models, however, one would also encounter the opposite scenario. *Garraffo et al.* [2001] found that the Lagrangian integral timescale of real drifters in the North Atlantic Ocean is typically 2 times smaller than that of synthetic drifters released in the flow field from a realistic high-resolution Miami Isopycnic Ocean Model. Some ocean circulation models tend to be less energetic than the real ocean, in part due to errors in wind forcing (e.g., use of climatological versus daily winds). Therefore, another experiment is carried out (EXP-FORCE2), in which drifter data from EXP-BASE are assimilated into a model run driven by 50% smaller wind forcing (i.e., the strength of the Sverdrup circulation is about 15 Sv). Due to weak wind forcing, the midlatitude jet in this experiment is stable, and the flow field is steady (Figure 7a) such that assimilation experiment at t = 0 is the same as no-assimilation case at all times. Once the assimilation of drifters positions is carried out, both the intensity and location of the mesocale eddy activity is reproduced successfully, and the velocity error

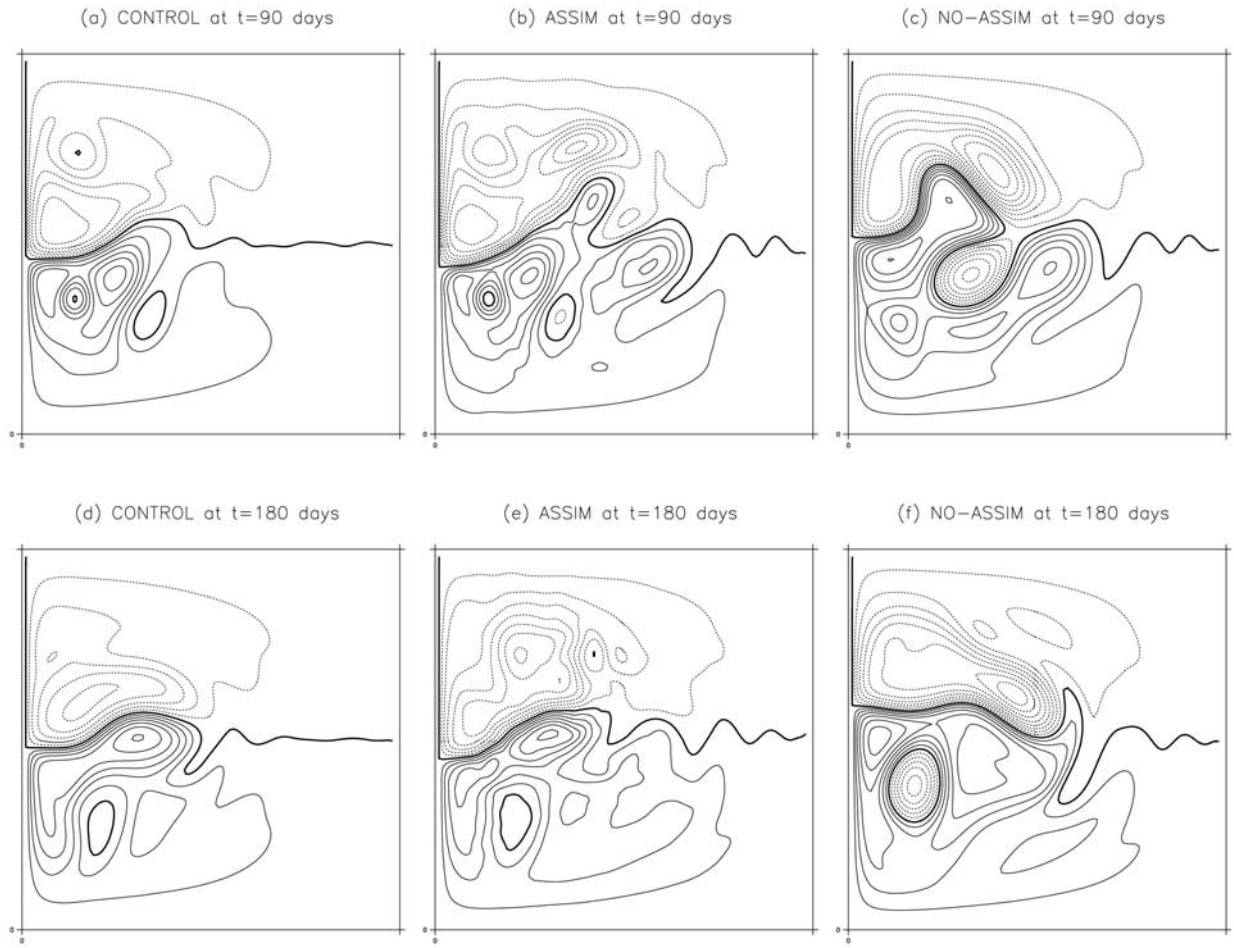

Figure 6. Transport stream function (ci: 10 Sv) for control run, assimilation run (using Δt = 2 days), and no-assimilation run at t = 90 days (a–c) and at t = 180 days (d–f) in EXP-FORCE1.

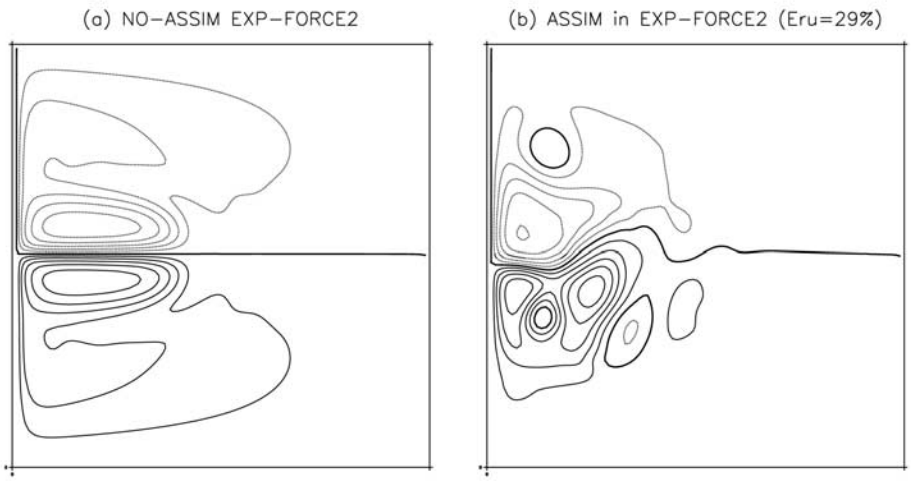

Figure 7. Transport stream function for (a) no-assimilation run (ci: 5 Sv) and (b) assimilation run (ci: 10 Sv) at t = 90 days (a–c) in EXP-FORCE2. Refer to Figures 5a and 6a for the control flow field at t = 90 days. The error between control and assimilation is *Eru* = 29% at t = 90 days.

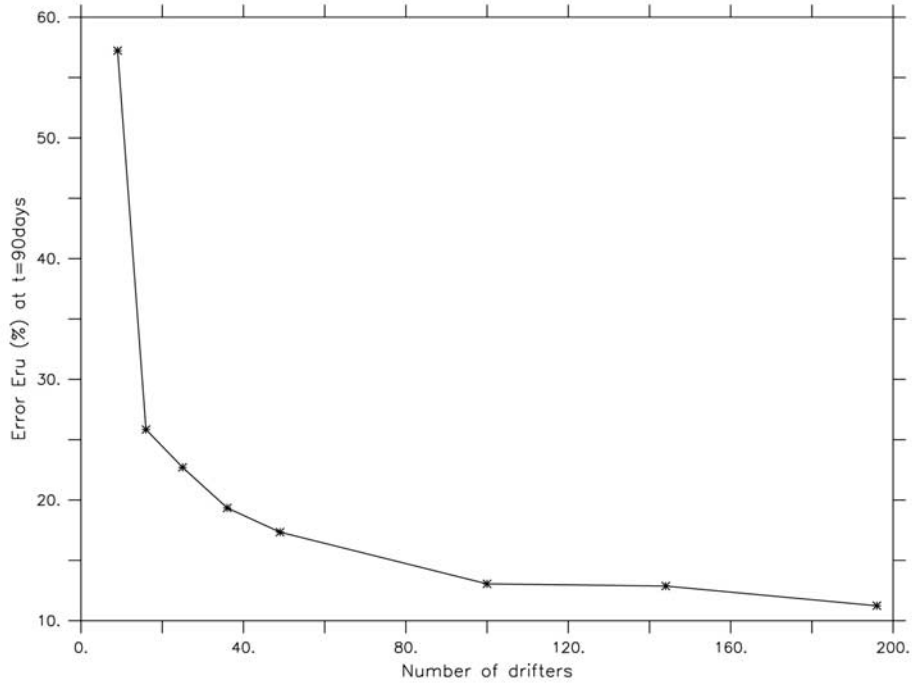

Figure 8. Convergence error *Eru* (%) at t = 90 days as a function of the number of drifters from experiments EXP-DRIFT-9–196.

between flow fields of control (e.g., Figures 5a and 6a) and assimilation (Figure 7b) cases is *Eru* = 29% at t = 90 days.

[49] These results indicate that the drifter assimilation is effective in the presence of large errors in the wind forcing driving the ocean circulation model.

4.4. Sensitivity to the Number of Drifters

[50] Seven experiments, in addition to EXP-BASE, have been performed with 9, 16, 36, 49, 100, 144, and 196 drifters homogeneously released in the energetic western midlatitude jet region (Figure 3a), while keeping other model parameters same as those in EXP-BASE (Table 2). The velocity error *Eru* at t = 90 days is plotted as a function of the number of drifters in Figure 8, which shows the asymptoting behavior of error as the number of drifters is increased. The error is about *Eru* = 11% with 196 drifters, but only two percentage points higher with 100 drifters. Visually, the difference in the flow field between assimilation and control cases is not noticeable when the number of drifters exceeds 25. There is significant increase in error only when the number of drifters is reduced to 9. However, many features of the mesoscale eddy field in the control experiment are reproduced well with 16 and even with 9 drifters in the assimilation run (Figure 9). This result indicates that the assimilation is effective even with a limited number of instruments, and it is quite encouraging, especially considering that the total basin size is 2000 × 2000 km^2.

4.5. Sensitivity to the Initial Distribution of Drifters

[51] In order to explore the impact of the launch location of the drifters on the assimilation error, 6 experiments are conducted, in which 25 drifters distributed over the same area as in EXP-BASE are moved around the domain according to the kinetic energy distribution (EXP-DRIFT-25b–g) as shown in Figure 10 (upper panel). EXP-BASE is identical to EXP-DRIFT-a. Also, an experiment is carried out, in which 25 drifters are launched homogeneously over the entire domain (EXP-DRIFT-25h). The error *Eru* at t = 90 days is then plotted as a function of the average kinetic energy of these subdomains normalized by that of the entire domain in Figure 10 (lower panel). This figure shows the general trend of better assimilation performance when the drifters are released in energetic regions. The importance of effectively sampling the energetic regions in assimilation problems has been pointed out in a number of previous studies [*Malanotte-Rizzoli and Holland*, 1988]. Notice that, despite the clear general trend, a considerable scatter can be seen in the results of Figure 10 (lower panel). This appears to be indicative of the sensitivity of Lagrangian motion to the detailed characteristics of the flow field, suggesting that other factors than the initial launching position play an important role, such as for instance dispersion and data voids occurring during the drifter history. The comprehensive investigation of optimal sampling for Lagrangian data assimilation described in this study is a difficult task beyond the scope of the present study. A recent paper by *Poje et al.* [2002] provides detailed considerations for drifter launch strategies to reconstruct Eulerian model flow fields using a least squares minimization of the difference between model and drifter velocities, as described by *Toner et al.* [2001a, 2001b].

[52] For applications in the real ocean, the results generally indicate the importance of the initial sampling strategy and suggest that a sampling targeted at high-energy regions is likely to be more efficient than a homogeneous sampling. Also, the results suggest that the assimilation can

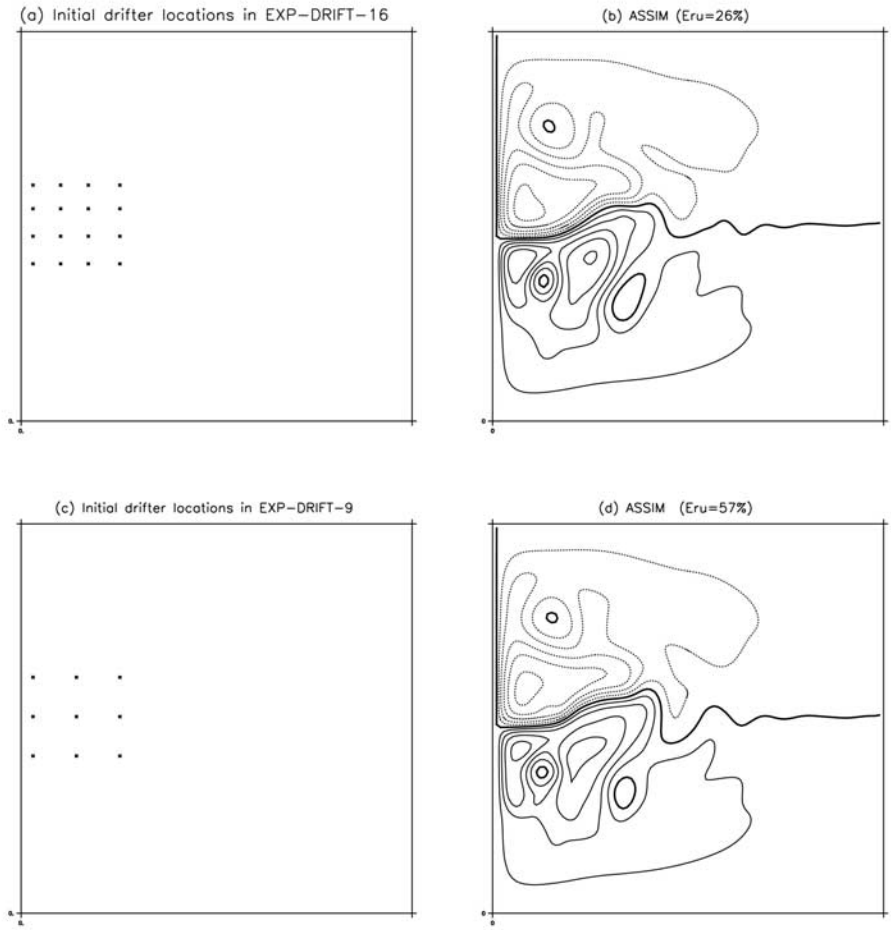

Figure 9. Initial drifter locations (a and c) and transport stream function (ci: 10 Sv) at $t = 90$ days (b and d) in EXP-DRIFT-16 and EXP-DRIFT-9, respectively.

be highly effective even with a relatively low data density, provided that the drifters are concentrated in the energetic regions. It should be pointed out, however, that the residence time of the drifters in the energetic structures might be significantly different in the model and in the real ocean. In the model, drifters released in the western recirculation tend to be trapped for a relatively long time (on the order of months), whereas in the real ocean (especially at the surface) drifters tend to be advected away from the energetic regions much quicker. As a consequence, the sampling problem in the ocean is certainly more complex, and probably implies repeated samplings in order to maintain a certain data density in the regions of interest.

4.6. Comparison With "Pseudo-Lagrangian" Assimilation

[53] A series of experiments has been performed in order to compare the results obtained with the Lagrangian assimilation with results from the pseudo-Lagrangian assimilation (section 2.2). To this end, the experiments discussed in sections 4.1 and 4.2, corresponding to the EXP-BASE configuration with various Δt, have been repeated using the pseudo-Lagrangian assimilation (EXP-PSEUDO) (see Table 2). In these experiments a bilinear spatial interpolation is used to find the Eulerian velocity at the drifter position. The pseudo-Lagrangian assimilation, as already noted in the Introduction, is often used in the assimilation of Lagrangian data [*Ishikawa et al.*, 1996], so that the comparison is of interest for practical applications.

[54] A guidance to the comparison is already given by the theoretical results of section 2.3, where error estimates for the two formulations are computed. For the pseudo-Lagrangian assimilation (9), the error computed over a time interval Δt and for a given grid point is expressed by

$$Er_{pseudo} = \| \tilde{\mathbf{u}}^a - \mathbf{u}^o \| \approx \| \mathbf{D}^o \mathbf{u}^o \| \qquad (20)$$

with $\mathbf{D}$ given by (13). Expression (20) indicates that the error is always finite as long as $\mathbf{D}^o\mathbf{u}^o$ is finite, i.e., Δt and $\Delta\mathbf{u}^o$ are finite. This suggests the existence of a bias that prevents the convergence of the assimilation to the control. This is not the case for the fully Lagrangian error (19), as discussed in section 4.2.

[55] The significance of the theoretical estimates (19) and (20) have been tested considering a set of experiments, in which the assimilation run starts from the same initial conditions as the control. According to (19) and (20), the

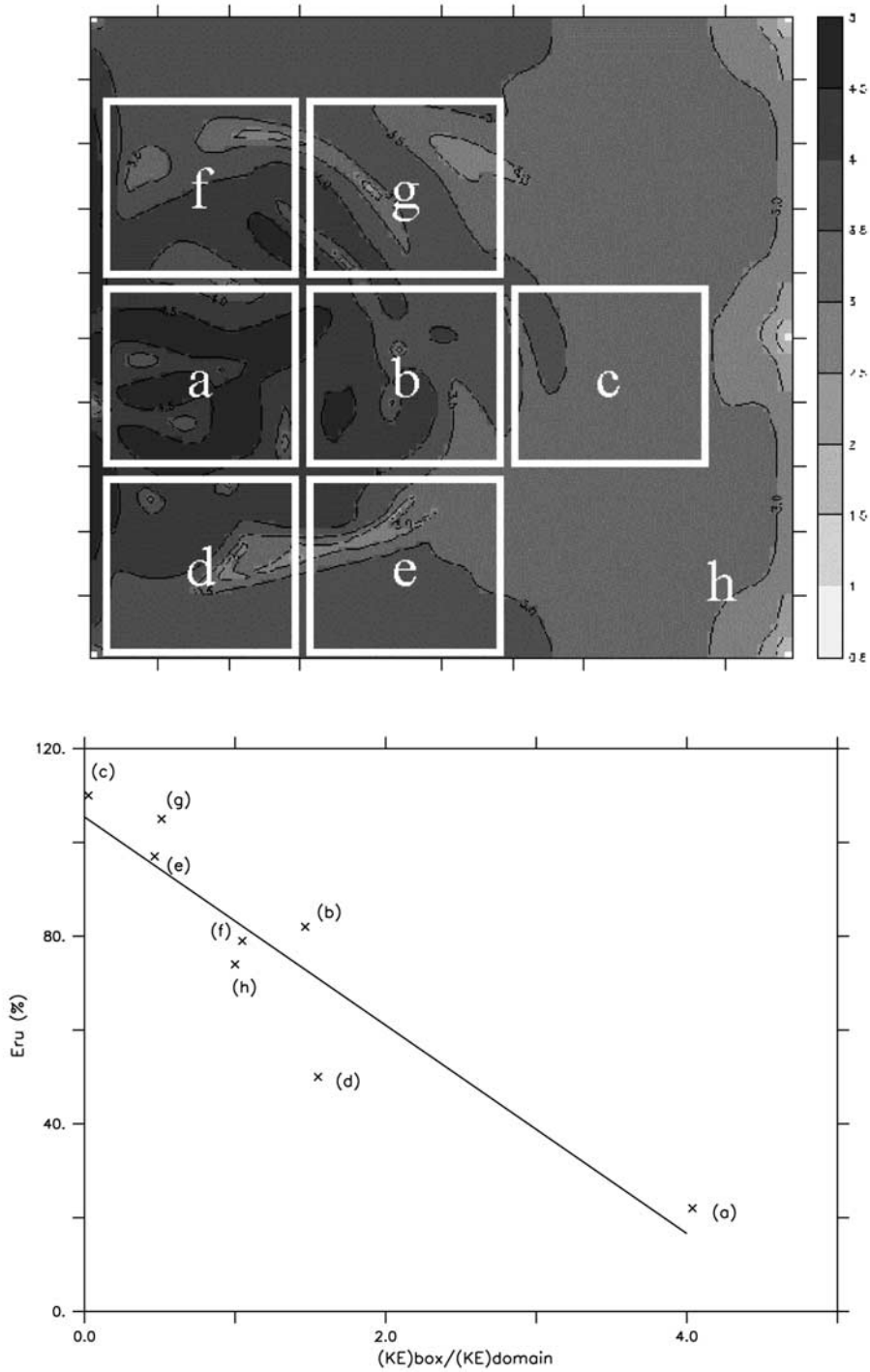

Figure 10. (Upper panel) Initial locations of the 25 drifters released in a box of 600 × 600 km^2 in experiments EXP-DRIFT-25a–g and EXP-DRIFT-25h, in which 25 drifters are homogeneously released in the 2000 × 2000 km^2 basin. The contours in the background denote $log(KE\ [cm^2\ s^{-2}])$ at $t = 0$. (Lower panel) Convergence error *Eru* (%) at t = 90 days from these experiments as a function of the spatial average of the kinetic energy in the launch box normalized by the basin-averaged kinetic energy. The solid line represents a least squares fit to data.

Lagrangian assimilation should have zero error, while the pseudo-Lagrangian assimilation should have a finite error (proportional to Δt). The experiments confirm that the Lagrangian error is indeed significantly smaller than the pseudo-Lagrangian error, especially for sizable Δt. As an example, for 10 day experiments, the Lagrangian *Eru* $\approx$ 0.8% using Δt = 2 days (nonzero due to numerical noise discussed above), while the pseudo-Lagrangian error is

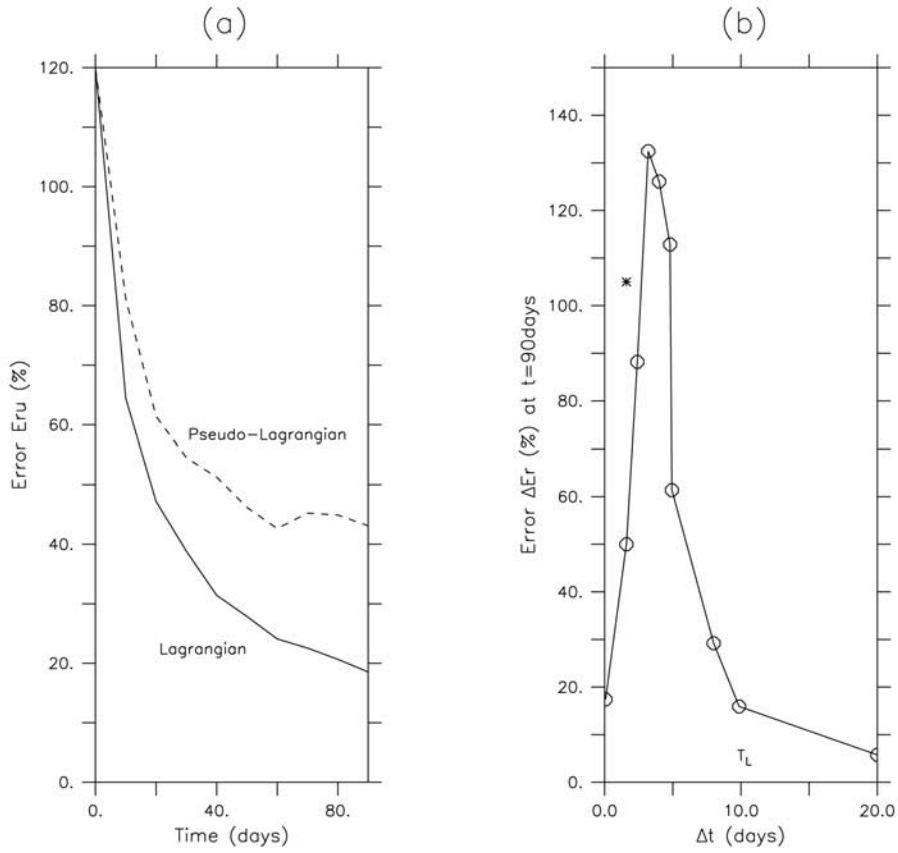

Figure 11. (a) Typical convergence error $Eru(t)$ (%) using fully Lagrangian (solid line) and pseudo-Lagrangian (dashed line) assimilation schemes. (b) Normalized error difference between Lagrangian and pseudo-Lagrangian methods, $\Delta Er(t = 90$ days) as a function of assimilation period Δt. The normalized error difference between the fully Lagrangian method and the assimilation of current meter data is marked by (*). The Lagrangian timescale is $T_L = 10$ days.

significantly higher (more than 1 order of magnitude), $Eru_{pseudo} \approx 11\%$.

[56] When the assimilation is performed starting from a different initial condition than the control, (19) and (20) do not provide direct indications on which scheme performs better, at least at initial times. The comparison between the EXP-BASE and the EXP-PSEUDO results shows that the Lagrangian assimilation performs better in all the considered cases. A typical example (for $\Delta t = 3$ days) of error evolution for Lagrangian and pseudo-Lagrangian assimilation schemes is shown in Figure 11a, which indicates that the error associated with the Lagrangian scheme is less than that for the pseudo-Lagrangian scheme and the difference increases in time. The value of the difference, or equivalently of the ratio $r(14)$ between Lagrangian and pseudo-Lagrangian errors, appears to change with Δt.

[57] A normalized error difference is defined as

$$\Delta Er = \frac{Eru_{pseudo} - Eru}{Eru}, \tag{21}$$

and the dependence of ΔEr, computed at $t = 90$ days, on Δt is depicted in Figure 11b. When Δt is very small (few hours to 1 day) the relative error ΔEr is small, showing that the two assimilation methods are giving similar results. For small sampling period, the approximation made by the pseudo-Lagrangian method (Lagrangian velocity approximated by Eulerian velocity) is valid, so the two methods are improving the velocity forecast with the same efficiency. ΔEr shows positive and increasing values for increasing Δt up to $\Delta t = 3$ days, i.e., $\approx T_L/3$. Here ΔEr reaches its maximum, $\Delta Er \approx 130\%$, indicating that the pseudo-Lagrangian error is more than the double of the Lagrangian error. For $\Delta t > 3$ days, ΔEr starts to decrease. There is an optimal range, 2 days $< \Delta Er <$ 5 days where $\Delta Er > 60\%$, showing that the direct use of the drifter position leads to a great improvement of the assimilation with respect to the more traditional pseudo-Lagrangian method. For $\Delta t \approx T_L$, ΔEr reduces, even though it is still positive and significant, $\Delta Er \approx 20\%$. This is likely to be due to the fact that the Lagrangian assimilation converges more efficiently to the control once the model reaches a condition that is relatively similar to it (20). For $\Delta t \approx T_L$, the model solution maintains quite distant from the control and this effect plays a less significant role. Finally, for $\Delta t \gg T_L$, ΔEr tends to zero as both Lagrangian and pseudo-Lagrangian errors reach approximately 90%.

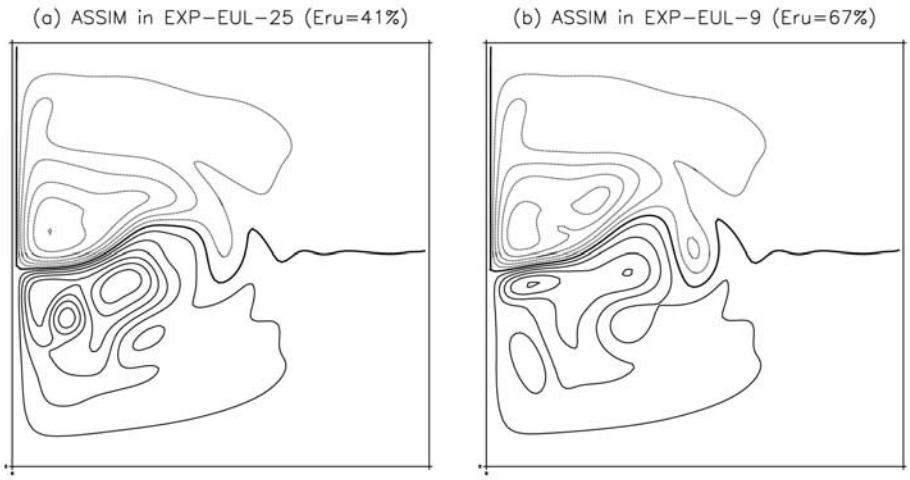

Figure 12. Transport stream function (ci: 10 Sv) at t = 90 days for (a) assimilation run with 25 current meters, EXP-EUL-25 and (b) assimilation run with 9 current meters, EXP-EUL-9.

[58] In summary, the results indicate that the pseudo-Lagrangian assimilation is subject to a bias, which is intimately related to the basic approximation of the Lagrangian velocity as Eulerian velocity. This is an unwanted property for an assimilation scheme. The Lagrangian velocity is not affected by this bias, and therefore is preferable in general. For practical applications, the Lagrangian assimilation provides significantly better results than the pseudo-Lagrangian assimilation in all cases, especially in the optimal range $T_L/5 < \Delta t < T_L/2$.

4.7. Comparison With Current Meter Assimilation

[59] A last series of experiments have been performed in order to compare the assimilation of drifter data to the assimilation of Eulerian velocity data at fixed points. The goal is to investigate how effective are the Lagrangian data compared to current meter data in correcting the velocity field, and to provide suggestions for monitoring and sampling strategies.

[60] Two experiments have been performed, in which "current meter" measurements, instead of drifter measurements, are assimilated. The experiments, EXP-EUL-25 and EXP-EUL-9 (Table 2), have the same configuration as EXP-BASE and EXP-DRIF-9 respectively, and are characterized by 25 and 9 current meters located in the central western region, with positions corresponding to the drifter initial conditions (Figures 3a and 7c). The assimilation of the Eulerian velocity is performed using the same local approximation as in the Lagrangian assimilation. In the case of current meters located at grid points, the algorithm is given by:

$$\mathbf{u}^a_{ij}(n) = \mathbf{u}^b_{ij}(n) + \alpha^{-1}\gamma_{ijm}\left(\mathbf{u}^o_{ij}(n) - \mathbf{u}^b_{ij}(n)\right). \qquad (22)$$

The results are shown in Figure 12 for Δt = 2 days, with snapshots of the assimilation at t = 90 days to be compared with the control and no assimilation in Figures 3n and 3p. Other Δt values have also been considered and a trend of $Eru(\Delta t)$ qualitatively similar to the one in Figure 4 has been found, even though the error increases more slowly at increasing Δt. This is because the Eulerian velocity measurements are instantaneous and do not deteriorate with increasing Δt as in the Lagrangian case.

[61] The results with 25 current meters (EXP-EUL-25) show a good qualitative resemblance with the control. Compared to the results with 25 drifters (EXP-MAIN) (Figure 3o), the stream function field from day 90, EXP-EUL-25 appears more similar to the no assimilation case, especially in regions where there are no measurements, and the error is significantly higher (41% instead than 18%). The normalized error difference between the fully Lagrangian method and the assimilation of current meter data was computed and ΔEr_{Eul} = 103% (marked in Figure 11b by "*") showing that the relative improvement with respect to the pseudo-Lagrangian case is greater.

[62] This is even more evident when the number of instruments is decreased, as in EXP-EUL-9. In this case the stream function appears modified only in a few areas and it is characterized by a high error ($Eru \approx 67\%$). By comparison the results with 9 drifters (EXP-DRIF-9) (Figure 7d) appear much smoother and closer to the control ($Eru \approx 50\%$). This is likely to be due to the fact that the Lagrangian instruments are moving and give informations in space and time, while current meters yield informations only at fixed points, leading to error accumulation in regions with no data.

[63] In summary, the results indicate that the assimilation of Lagrangian data is more effective than the assimilation of current meter data, especially in the case of low instrument density. One remark, already made earlier, is that in the ocean the residence time of Lagrangian instruments in energetic regions might be lower than in the model, so that the use of fixed instruments may be more convenient in some key areas.

5. Summary and Concluding Remarks

[64] In light of the increasing number of Lagrangian instruments released in the ocean, and of the recent advan-

ces in the realism of ocean general circulation models toward oceanic forecasting, the problem of assimilation of positions of Lagrangian instruments in Eulerian models is investigated. A general formulation specifically written for the position variables is introduced, and a simplified algorithm has been derived and tested numerically. This algorithm is characterized by an approximation of the sensitivity matrix, $\mathbf{G} = \delta\mathbf{H}/\delta u(2)$, based on a zeroth-order expansion of the position increments $\Delta\,\mathbf{r}$, so that the velocity gradient is not explicitly included. Only one assimilation time step Δt, or equivalently two successive data points, are considered so that the assimilation is written in terms of Lagrangian velocity $\mathbf{v}$, i.e., velocity averaged along particle trajectories during Δt. Even though the simplified algorithm is the focus of the present paper, higher-order generalizations, able to include the full path information in the assimilation, are also discussed, and a two time step algorithm is explicitly derived.

[65] We emphasize that the algorithm (5) introduced in this paper is not only highly portable, and easy to code, it is also computationally highly efficient. Therefore, this technique presents significant advantages in implementation and computational efficiency with respect to the alternative approach used by *Kamachi and O'Brien* [1995], who relied on an adjoint model, which requires significant coding for each ocean model, and additional integration time.

[66] Note that the Lagrangian assimilation, even in the one-step approximation, is different from the pseudo-Lagrangian approximation often used in the literature. In the Lagrangian assimilation, the position increments $\Delta\mathbf{r}$ of the floats during Δt are forecasted by the model, and the model Eulerian velocity is corrected considering the difference between forecasted and observed increments (or equivalently between forecasted and observed Lagrangian velocities $\mathbf{v} = \Delta\mathbf{r}/\Delta t$). In the pseudo-Lagrangian case, instead, $\Delta\mathbf{r}$ is not forecasted by the model and the correction term depends on the difference between Eulerian model velocities $\mathbf{u}^b$ and observed Lagrangian velocities $\mathbf{v}^o$. The two approaches are expected to coincide only in the limit of small Δt, when Lagrangian and Eulerian velocities coincide.

[67] The Lagrangian assimilation algorithm has been tested using the twin experiment approach with a reduced gravity, quasi-geostrophic model using a double-gyre configuration. A base experiment has been tested first, in which 25 drifters launched in the western central region of the control run are assimilated in the assimilation run, characterized by a different initial condition. The assimilation is highly effective, showing a significant convergence toward the control in the first 3 months. The stream function patterns of the solutions are nearly identical, while the error computed as RMS velocity of the difference is $Eru \approx 20\%$ at 90 days. The robustness of these results has been tested by varying a number of parameters, such as the sampling period Δt, the wind forcing, and the drifter number and initial conditions. The parameters are varied in a realistic range, so that the results can provide guidance for ocean applications. A list of the errors for all the test simulations is summarized in Table 3.

[68] The primary new contribution of this study to improve our understanding of how to better utilize Lagrangian nature of drifter data in ocean models is that it is shown that the difference in effectiveness between pseudo-Lagrangian and fully Lagrangian assimilation is only a function of the assimilation period Δt scaled by the Lagrangian decorrelation timescale T_L, and quantified this difference. The results at varying Δt show the existence of an optimal range, $\Delta t \approx T_L/5$, with Eru (90 days) < 20%. For the ocean surface, using appropriate scaling by T_L, this corresponds to $\Delta t \approx 5-15$ hours, while for the subsurface $\Delta t \approx 1.5-2$ days. Even for longer Δt, the assimilation remains effective, with $Eru \approx 38\%$ for $\Delta t \approx T_L/2$ (0.5–1.5 days for the surface, 3.5–7 days for subsurface) and $Eru \approx 65\%$ for $\Delta t \approx T_L$. For $\Delta t > T_L$, the information content on the Eulerian velocity that can be obtained from the positions degrades and the assimilations loses its effectiveness. This result complements those by *Kamachi and O'Brien* [1995], who conducted experiments using a single Δt, in that we isolate when the Lagrangian assimilation is more effective than classical techniques, and when it is not necessary to try to incorporate Lagrangian considerations in assimilation schemes.

[69] The impact of the uncertainties in the oceanic forcing functions on the assimilation is investigated by forcing the assimilation run by winds of different intensity than that in the control. The results are encouraging. The method is able to correct the model forecast in both cases when the wind forcing is over estimated or under estimated. Varying the number of drifters and their initial sampling shows that the assimilation is effective even with a small number of drifters (9 drifters for a basin of 2000×2000 km^2), provided that they are concentrated in the energetic regions. When the drifters are released in high-energy regions (meandering jet, recirculation regions), and their residence time in those regions is high, the success of the assimilation is guaranteed. In the real ocean, the sampling strategy might be more complex, including repeated samplings, given that the residence time in the energetic structures is likely to be smaller than in the model, so that other factors may be important like dispersion and data voids.

[70] The results obtained with the Lagrangian assimilation have then been compared with other assimilation methods. Regarding the pseudo-Lagrangian assimilation, it has been found that it is affected by a bias, directly related to its basic assumption. In practical applications, the Lagrangian assimilation provides better results in all the tested cases, and especially in the optimal range $\Delta t \leq T_L/2$. The assimilation of current meters (fixed-point velocity instruments), instead of drifters, has also been tested. It is found that the Lagrangian assimilation is more effective, especially for low density values, since Lagrangian instruments tend to provide a smoother and more homogeneous coverage avoiding error accumulation in regions of data voids.

[71] In summary, the results are very positive and indicate the high potential of using Lagrangian data for assimilation in Eulerian models. The present results can be considered as a first step in the investigation, since they are obtained using the simplest one-step local algorithm and they are applied to the quasi-geostropic dynamics. Future work is planned to generalize the present work considering more complex algorithms to compute $\mathbf{G}$ and applying the methodology to the more complete primitive equation models. Regarding the use of multistep algorithm, allowing the more complete

use of path information, an important issue will be to verify whether or not the increased values of the Lagrangian data will compensate the increased complexity in the assimilation algorithm, and how many successive steps will be optimal to consider, in relation also to the intrinsic Lagrangian timescale of the processes. Also, realistic problems associated with specific instruments will be considered. As an example, in the case of profiling floats, the position information is expected to depend not only on the motion experienced at the reference level but also on the drift experienced during the ascendant motion. This implies that the information on the velocity at the reference level are contaminated by vertical shear. How to take into account this contamination and possibly remove it is an important open issue for Lagrangian assimilation applications.

Appendix A: Derivation of Assimilation Formulas

[72] The derivation of (5) from (1) and (2) requires three steps:

1. Relate Lagrangian data to Eulerian model variables;
2. Find an appropriate representation for **G**; and
3. Parameterize $\mathbf{R}^b$ and $\mathbf{R}^o$ in a parsimonious way.

[73] (1) Let grid indices vary in the following ranges $i = 1{:}I$, $j = 1{:}J$, so $K = IJ$ is the number of grid points, time indices vary $n = 1{:}N$, and particles are numbered $m = 1{:}M$. Define the observational functional $\mathbf{H}(\mathbf{u}^b)$ as a $2MN$ column vector

$$\mathbf{H}(\mathbf{u}^b) = \left(\mathbf{v}_1^b(1), \mathbf{v}_2^b(1), \ldots, \mathbf{v}_M^b(1), \mathbf{v}_1^b(2), \mathbf{v}_2^b(2), \ldots, \mathbf{v}_M^b(2), \ldots, \cdot \mathbf{v}_1^b(N), \mathbf{v}_2^b(N), \ldots, \mathbf{v}_M^b(N)\right)^T. \tag{A1}$$

Thus, we first list the Lagrangian velocities corresponding to the first time moment, then the second and so on. Also, $\mathbf{v}_1^b(1)$ means both components of this vector written in a row. In the same manner the observation vector is presented

$$\mathbf{y} = \left(\mathbf{v}_1^o(1), \mathbf{v}_2^o(1), \ldots, \mathbf{v}_M^o(1), \mathbf{v}_1^o(2), \mathbf{v}_2^o(2), \ldots, \mathbf{v}_M^o(2), \ldots, \cdot \mathbf{v}_1^o(N), \mathbf{v}_2^o(N), \ldots, \mathbf{v}_M^o(N)\right). \tag{A2}$$

Introduce the following elementary blocks (2×2 matrices)

$$\mathbf{g}_{m,ij}(n,k) \equiv \frac{\delta \mathbf{v}_m^b(n)}{\delta \mathbf{u}_{ij}^b(k)} \tag{A3}$$

and

$$\mathbf{R}^b_{i_1 j_1; i_2 j_2}(k_1,k_2) = \left\langle \mathbf{u}''_{i_1 j_1}(k_1) \mathbf{u}''_{i_2 j_2}(k_2)^T \right\rangle, \qquad \mathbf{R}^o_{m_1 m_2}(k_1,k_2) = \left\langle \mathbf{v}''_{m_1}(k_1) \mathbf{v}''_{m_2}(k_2)^T \right\rangle, \tag{A4}$$

where the double primes mean model and observational errors, respectively. The rows in these matrices correspond to the same velocity components. More exactly, the first row refers to the zonal component and the second row to the meridional component. The defined 2×2 matrices are used to build matrices **G**, $\mathbf{R^b}$, and $\mathbf{R^o}$ respectively included in (1). Matrix

$$\mathbf{L} \equiv \mathbf{G}\mathbf{R^b}\mathbf{G^T} + \mathbf{R^o} \tag{A5}$$

appearing in (1) is also represented through elementary blocks

$$\mathbf{L} = \begin{pmatrix} \mathbf{l}_{11}(1,1) & \ldots & \mathbf{l}_{1M}(1,1) & & \mathbf{l}_{11}(1,N) & \ldots & \mathbf{l}_{1M}(1,N) \\ \ldots & \ldots & \ldots & \ldots & \ldots & \ldots & \ldots \\ \mathbf{l}_{M1}(1,1) & \ldots & \mathbf{l}_{MM}(1,1) & & \mathbf{l}_{M1}(1,N) & \ldots & \mathbf{l}_{MM}(1,N) \\ & \ldots & & \ldots & & \ldots & \\ \mathbf{l}_{11}(N,1) & \ldots & \mathbf{l}_{M1}(N,1) & & \mathbf{l}_{11}(N,N) & \ldots & \mathbf{l}_{1M}(N,N) \\ \ldots & \ldots & \ldots & \ldots & \ldots & \ldots & \ldots \\ \mathbf{l}_{M1}(N,1) & \ldots & \mathbf{l}_{MM}(N,1) & & \mathbf{l}_{M1}(N,N) & \ldots & \mathbf{l}_{MM}(N,N) \end{pmatrix} \tag{A6}$$

where

$$\mathbf{l}_{m_1 m_2}(n_1,n_2) = \sum_{k_1,k_2,i_1,i_2,j_1,j_2} \mathbf{g}_{m_1,i_1 j_1}(n_1,k_1) \mathbf{R}^b_{i_1 j_1; i_2 j_2}(k_1,k_2) \mathbf{g}_{m_2,i_2 j_2} \cdot (n_2,k_2)^T + \mathbf{R}^o_{m_1 m_2}(n_1,n_2). \tag{A7}$$

Notice that **L** is of $2MN \times 2MN$ dimension, while **G** and $\mathbf{R^b}$ have dimensions of $2MN \times 2KN$ and $2KN \times 2KN$, respectively. Now (A3), (A4), (A5), and (A7) makes (1) a computational tool since they contain exactly defined vectors and matrices. A remaining problem is that the blocks defined in (A3) and (A4) are not parameterized yet and the dimension of **L** may be too large for efficient inversion.

[74] (2) First, we show that the variational derivative of the displacement with respect to the Eulerian velocity is given by

$$\frac{\delta \mathbf{r}(t)}{\delta \mathbf{u}(s,\mathbf{r})} = \exp\left(\int_s^t \frac{D\mathbf{u}}{D\mathbf{r}}(\tau) d\tau \right) \theta(t-s) \cdot \delta(\mathbf{r}(s) - \mathbf{r}), \tag{A8}$$

where $\theta(t)$ is the Heaviside step function, $\delta(\mathbf{r})$ is the Dirac delta function, and $(D\mathbf{u}/D\mathbf{r})(\tau)$ is the Eulerian velocity gradient (2×2 matrix) taken at the $(\tau,\mathbf{r}(\tau))$. It is important to notice that the integral in (A8) is understood as a multiplicative integral, i.e., (A8) means that

$$\frac{\delta r^k(t)}{\delta u^l(s,\mathbf{r})} = a_{kl}(t,s) \theta(t-s) \delta(\mathbf{r}(t) - \mathbf{r}), \tag{A9}$$

where r^k and $u^l(s, \mathbf{r})$ are components of the position and velocity vectors, respectively, and $a_{kl}(t, s)$ satisfy

$$\frac{\partial a_{kl}(t,s)}{\partial t} = \sum_j \frac{\partial u_k}{\partial r_j}(t) a_{jl}(t,s), a_{kl}(s,s) = \delta_{kl}. \tag{A10}$$

Let us prove (A9) and (A10). Taking the variational derivative of both parts of

$$\frac{d\mathbf{r}}{dt} = \mathbf{u}(t, \mathbf{r}(t))$$

one gets

$$\frac{d}{dt} \frac{\delta \mathbf{r}(t)}{\delta \mathbf{u}(s,\mathbf{r})} = \frac{\delta \mathbf{u}(t,\mathbf{r}(t))}{\delta \mathbf{u}(s,\mathbf{r})} = \delta(t-s)\delta(\mathbf{r}(t) - \mathbf{r}) + \frac{D\mathbf{u}}{D\mathbf{r}}(t) \frac{\delta \mathbf{r}(t)}{\delta \mathbf{u}(s,\mathbf{r})}.$$

Integrating the last equation with the zero initial conditions we obtain (A9) and (A10).

[75] In particular, (A8) implies

$$\frac{\delta \mathbf{r}(t)}{\delta \mathbf{u}(t,\mathbf{r})} = \mathbf{I}\delta(\mathbf{r}(t)-\mathbf{r}) \tag{A11}$$

and for small Δt

$$\frac{\delta \mathbf{r}(t+\Delta t)}{\delta \mathbf{u}(t,\mathbf{r})} = \delta(\mathbf{r}(t)-\mathbf{r})\left(\mathbf{I}+\Delta t\frac{D\mathbf{u}}{D\mathbf{r}}(t)\right), \tag{A12}$$

where $\mathbf{I}$ is the unit 2×2 matrix. Then, for observations discrete in space we use the following approximation of the delta function in (A9), (A11), and (A12)

$$\delta(\mathbf{r}) \approx \frac{1}{h^2}E_h(x,y),$$

where E_h is defined in (6). Thus, for $n \geq k$

$$\frac{\delta \mathbf{r}_m(n)}{\delta \mathbf{u}_{ij}(k)} = \Delta t E_h(x_m(k)-ih, y_m(k)-jh)\mathbf{A}_{nk},$$

where

$$\mathbf{A}_{nk} = \left(a_{ij}(n\Delta t, k\Delta t)\right)$$

and

$$\frac{\delta \mathbf{r}_m(n)}{\delta \mathbf{u}_{ij}(k)} = 0, \tag{A13}$$

otherwise. Hence, for $n \geq k$ the entries of $\mathbf{G}$ introduced in (A3) are given by

$$\mathbf{g}_{m,ij}(n,k) \equiv \frac{\delta \mathbf{v}_m(n)}{\delta \mathbf{u}_{ij}(k)} = E_h(x_m(k)-ih, y_m(k)-jh)\left(\mathbf{A}_{nk}-\mathbf{A}_{n-1,k}\right). \tag{A14}$$

In particular

$$\mathbf{g}_{m,ij}(n,n) \equiv \frac{\delta \mathbf{v}_m(n)}{\delta \mathbf{u}_{ij}(n)} = E_h(x_m(n)-ih, y_m(n)-jh)\mathbf{I}, \tag{A15}$$

$$\mathbf{g}_{m,ij}(n+1,n) \equiv \frac{\delta \mathbf{v}_m(n+1)}{\delta \mathbf{u}_{ij}(n)} = E_h(x_m(n)-ih, y_m(n)-jh) \cdot \frac{D\mathbf{u}}{D\mathbf{r}}(n\Delta t), \tag{A16}$$

where $\mathbf{I}$ is 2×2 unit matrix.

[76] (3) We assume that the errors of both model and observed variables are uncorrelated in time and space, i.e.,

$$\mathbf{R}^b_{i_1 j_1; i_2 j_2}(k_1,k_2) = \sigma_b^2 \mathbf{I}\delta_{i_1 i_2}\delta_{j_1 j_2}\delta_{k_1 k_2}, \tag{A17}$$

and

$$\mathbf{R}^o_{m_1,m_2}(k_1,k_2) = \sigma_o^2 \mathbf{I}\delta_{m_1 m_2}\delta_{k_1 k_2}. \tag{A18}$$

From the mathematical viewpoint, consideration of more general covariances is not more difficult and possible implications of "nonwhite noise" errors have been briefly discussed in section 2.3. From a practical viewpoint, a more general covariance function would require the estimation of many more parameters.

[77] Under these assumptions, (A7) becomes

$$\mathbf{l}_{m_1 m_2}(n_1,n_2) = \sigma_b^2 \sum_{k,i,j} \mathbf{g}_{m_1,ij}(n_1,k)\mathbf{g}_{m_2,ij}(n_2,k)^T + \sigma_o^2 \delta_{n_1 n_2}\delta_{m_1 m_2}\mathbf{I}$$

and the assimilation formula (1) is approximated by

$$\mathbf{u}^a(n) = \mathbf{u}^b(n) + \sigma_b^2 \sum_{p,q} \mathbf{G}(p,n)^T \tilde{\mathbf{l}}(p,q)\left(\mathbf{v}^o(q)-\mathbf{v}^b(q)\right), \tag{A19}$$

where

$$\mathbf{u}^a(n) = \left(\mathbf{u}^a_{ij}(n)\right), \quad \mathbf{u}^b(n) = \left(\mathbf{u}^b_{ij}(n)\right), \mathbf{G}(p,n) = \left(\mathbf{g}_{m,ij}(p,n)\right),$$

$$\tilde{\mathbf{l}}(p,q) \equiv \left(\tilde{\mathbf{l}}_{m_1,m_2}(p,q)\right), \quad \mathbf{v}^o(q) = \left(\mathbf{v}^o_m(q)\right), \mathbf{v}^b(q) = \left(\mathbf{v}^b_m(q)\right),$$

$\tilde{l}_{m1m2}(n_1, n_2)$ are the 2×2 entries of $\mathbf{L}^{-1}$. Inversion of the matrix $\mathbf{L}$ is the main obstacle in practical application of (A19) since its dimension can be very large. However, if one assumes (4), then the inverse matrix can be easily found by the perturbation theory up to any order in ϵ. In particular for the zeroth-order approximation one get (5). Indeed, using condition (4) and relation (A15), we conclude that

$$\mathbf{G} \approx \mathbf{J} \tag{A20}$$

where

$$\mathbf{J} = \begin{pmatrix} \mathbf{J}(1) & 0 & \dots & 0 \\ 0 & \mathbf{J}(2) & \dots & 0 \\ \dots & \dots & \dots & \dots \\ 0 & \dots & \dots & \mathbf{J}(N) \end{pmatrix},$$

each $\mathbf{J}(n)$ is a $2M \times 2K$ matrix with entries

$$(\mathbf{J}(n))_{m,ij} = \gamma_{ijm}\mathbf{I},$$

γ_{ijm} is defined in (6). Notice that

$$\mathbf{J}\mathbf{J}^T \approx \mathbf{I}, \tag{A21}$$

where $\mathbf{I}$ is the $2MN \times 2MN$ unit matrix. From (A20), it follows that in the zeroth order of ϵ we have

$$\mathbf{R}^b\mathbf{G}^T\mathbf{L}^{-1} \approx \sigma_b^2\mathbf{J}^T\left(\sigma_b^2\mathbf{J}\mathbf{J}^T + \sigma_o^2\mathbf{I}\right)^{-1}.$$

With (A21) and (6), we readily get (5).

[78] To incorporate the observations made at the two previous moments, one should use the following two-diagonal approximation

$$\mathbf{G} \approx \mathbf{J} + 2\mathbf{D}\mathbf{J}, \quad \| \mathbf{D} \| \ll 1, \tag{A22}$$

instead of (A20), where

$$\mathbf{D} = \begin{pmatrix} 0 & 0 & \dots & \dots & 0 \\ \mathbf{D}(1) & 0 & 0 & \dots & 0 \\ 0 & \mathbf{D}(2) & \dots & \dots & 0 \\ \dots & \dots & \dots & \dots & \dots \\ 0 & 0 & \dots & \mathbf{D}(N-1) & 0 \end{pmatrix},$$

with $2K \times 2K$ entries given by

$$(\mathbf{D}(n))_{m_1 m_2} = \delta_{m_1 m_2} \mathbf{D}_{m_1}(n)$$

and $\mathbf{D}_m(n)$ is the matrix of velocity gradients (multiplied by $\Delta t/2$) at the position of the mth particle at moment n. Condition (A22) allows to easily find the inverse matrix $\mathbf{L}^{-1}$ up to the first order in $\mathbf{D}$ by using the perturbation theory arguments. With (A15) and (A16) in mind, this results in (15).

[79] **Acknowledgments.** The authors greatly appreciate the support of the Office of Naval Research under grants N00014-97-1-0620 and N00014-99-1-0049 (A. Molcard, A. Griffa, and T. M. Özgökmen), N00014-99-1-0042 (L. I. Piterbarg), and N00014-95-1-0257 and N00014-99-1-0049 (A. J. Mariano). The authors would like to thank Mike Chin, Nadia Pinardi, and Encho Demirov for many valuable discussions.

References

Arakawa, A., Computational design for long-term numerical integration of the equations of fluid motion: Two dimensional incompressible flow, part 1, *J. Comput. Phys.*, *1*, 119–143, 1966.

Bauer, S., M. S. Swenson, A. Griffa, A. J. Mariano, and K. Owens, Eddy-mean flow decomposition and eddy-diffusivity estimates in the tropical Pacific Ocean, *J. Geophys. Res.*, *103*, 30,855–30,871, 1998.

Bennett, A. F., *Inverse Methods in Physical Oceanography*, 346 pp., Cambridge Univ. Press, New York, 1992.

Berloff, P., and J. C. McWilliams, Material transport in oceanic gyres: part 2. Hierarchy of stochastic models, *J. Phys. Oceanogr.*, *32*(3), 797–830, 2002.

Cane, M. A., A. Kaplan, R. N. Miller, B. Tang, E. C. Hackert, and A. J. Busalacchi, Mapping tropical Pacific sea level: Data assimilation via a reduced state space Kalman filter, *J. Phys. Oceanogr.*, *101*, 22,599–22,617, 1996.

Carter, E. F., Assimilation of Lagrangian data into a numerical model, *Dyn. Atmos. Oceans*, *13*, 335–348, 1989.

Castellari, S., A. Griffa, T. M. Özgökmen, and P.-M. Poulain, Prediction of particle trajectories in the Adriatic Sea using Lagrangian data assimilation, *J. Mar. Syst.*, *29*, 33–50, 2001.

Chin, T. M., A. J. Mariano, and E. P. Chassignet, Spatial regression with Markov random fields for Kalman filter approximation in least-squares solution of oceanic data assimilation problems, *J. Geophys. Res.*, *104*, 1233–1257, 1999.

Chin, T. M., A. C. Haza, and A. J. Mariano, A reduced-order information filter for multi-layer shallow water models: Profiling and assimilation of sea surface height, *J. Atmos. Oceanic Technol.*, *9*, 517–533, 2002.

Coulliette, C., and S. Wiggins, Intergyre transport in a wind-driven, quasi-geostrophic double gyre: An application of lobe dynamics, *Nonlinear Process. Geophys.*, *7*, 59–85, 2000.

Davis, R. E., Observing the general circulation with floats, *Deep Sea Res.*, *38*, 5531–5571, 1991.

Evensen, G., D. P. Dee, and J. Schroter, Parameter estimation in dynamical models, in *Ocean Modeling and Parameterization*, edited by E. P. Chassignet and J. Veron, pp. 373–398, Kluwer Acad., Norwell, Mass., 1998.

Falco, P., A. Griffa, P.-M. Poulain, and E. Zambianchi, Transport properties in the Adriatic Sea deduced from drifter data, *J. Phys. Oceanogr.*, *30*, 2055–2071, 2000.

Fratantoni, D. M., North Atlantic surface circulation during the 1990's observed with satellite-tracked drifters, *J. Geophys. Res.*, *106*, 22,067–22,093, 2001.

Garraffo, Z. D., A. J. Mariano, A. Griffa, C. Veneziani, and E. P. Chassignet, Lagrangian data in a high-resolution numerical simulation of the North Atlantic, 1, Comparison with in situ drifter data, *J. Mar. Syst.*, *29*, 157–176, 2001.

Gazdag, J., Time-differencing schemes and transform methods, *J. Comput. Phys.*, *20*, 196–207, 1976.

Ghil, M. and P. Malanotte-Rizzoli, Data assimilation in meteorology and oceanography, in *Advances in Geophysics*, vol. 33, pp. 141–266, Academic, San Diego, Calif., 1991.

Griffa, A., Applications of stochastic particle models to oceanographic problems, in *Stochastic Modelling in Physical Oceanography*, edited by R. Adler, P. Muller, and B. Rozovskii, pp. 113–128, Birkhäuser Boston, Cambridge, Mass., 1996.

Griffa, A., K. Owens, L. Piterbarg, and B. Rozovskii, Estimates of turbulence parameters from Lagrangian data using a stochastic particle model, *J. Mar. Res.*, *53*, 212–234, 1995.

Holland, W. R., The role of mesoscale eddies in the general circulation of the ocean, *J. Phys. Oceanogr.*, *22*, 1033–1046, 1978.

Hernandez, F., P. Y. Le Traon, and N. H. Barth, Optimizing a drifter cast strategy with a genetic algorithm, *J. Atmos. Oceanic Technol.*, *12*, 330–345, 1995.

Ishikawa, Y. I., T. Awaji, and K. Akimoto, Successive correction of the mean sea surface height by the simultaneous assimilation of drifting buoy and altimetric data, *J. Phys. Oceanogr.*, *26*, 2381–2397, 1996.

Kamachi, M., and J. J. O'Brien, Continuous assimilation of drifting buoy trajectory into an equatorial Pacific Ocean model, *J. Mar. Syst.*, *6*, 159–178, 1995.

Lavender, K. L., R. E. Davis, and W. B. Owens, Direct velocity measurements in the Labrador and Irminger Seas describe pathways of Labrador Sea Water, *Nature*, *407*, 66–69, 2000.

Lorenc, A. C., A Bayesian approach to observation quality control in variational and statistical assimilation, paper-presented at Aha Huliko Hawaiian Winter Workshop, Univ. of Hawaii, Honolulu, Hawaii, 2000.

Malanotte-Rizzoli, P., and W. R. Holland, Data constraint applied to models of the ocean general circulation, part 2, The transient, eddy resolving case, *J. Phys. Oceanogr.*, *18*, 1093–1107, 1988.

Mariano, A. J., A. Griffa, T. M. Özgökmen, and E. Zambianchi, Lagrangian analysis and predictability of coastal and ocean dynamics, *J. Atmos. Oceanic Technol.*, *19*(7), 1114–1126, 2002.

Owens, W. B., A statistical description of the mean circulation and eddy variability in the northwestern Atlantic using SOFAR floats, *Progr. Oceanogr.*, *28*, 257–303, 1991.

Özgökmen, T. M., A. Griffa, L. I. Piterbarg, and A. J. Mariano, On the predictability of the Lagrangian trajectories in the ocean, *J. Atmos. Oceanic Technol.*, *17/3*, 366–383, 2000.

Özgökmen, T. M., L. I. Piterbarg, A. J. Mariano, and E. H. Ryan, Predictability of drifter trajectories in the tropical Pacific Ocean, *J. Phys. Oceanogr.*, *31*, 2691–2720, 2001.

Piterbarg, L. I., Short term prediction of Lagrangian trajectories, *J. Atmos. Oceanic Technol.*, *18*, 1398–1410, 2001.

Poje, A. C., and G. Haller, Geometry of cross-stream mixing in a double-gyre ocean model, *J. Phys. Oceanogr.*, *29*, 1649–1665, 1999.

Poje, A. C., M. Toner, A. D. Kirwan Jr., and C. K. R. T. Jones, Drifter launch strategies based on Lagrangian templates, *J. Phys. Oceanogr.*, *32*, 1855–1869, 2002.

Poulain, P.-M., Adriatic Sea surface circulation as derived from drifter data between 1990 and 1999, *J. Mar. Syst.*, *29*, 3–32, 2001.

Smith, R. D., M. E. Maltrud, F. O. Bryan, and M. W. Hecht, Numerical simulation of the North Atlantic ocean at 1/10°, *J. Phys. Oceanogr.*, *30*, 1532–1561, 2000.

Stammer, D., and E. P. Chassignet, Ocean state estimation and prediction in support of oceanographic research, *Oceanography*, *13*, 51–56, 2000.

Swenson, M. S., and P. P. Niiler, Statistical analysis of the surface circulation of the California Current, *J. Geophys. Res.*, *101*, 22,631–22,645, 1996.

Thomson, D. J., A random walk model of dispersion in turbulent flows and its application to dispersion in a valley, *Q. J. R. Meteorol. Soc.*, *112*, 511–529, 1986.

Toner, M., A. C. Poje, A. D. Kirwan, C. K. R. T. Jones, B. L. Lipphardt, and C. E. Grosch, Reconstructing basin-scale Eulerian velocity fields from simulated drifter data, *J. Phys. Oceanogr.*, *31*, 1361–1376, 2001a.

Toner, M., A. D. Kirwan, L. H. Kantha, and J. K. Choi, Can general circulation models be assessed and their output enhanced with drifter data?, *J. Geophys. Res.*, *106*, 19,563–19,579, 2001b.

Wiggins, S., *Chaotic Transport in Dynamical Systems*, 301 pp., Springer-Verlag, New York, 1992.

Zhang, H. M., M. D. Prater, and T. Rossby, Isopycnal Lagrangian statistics from the North Atlantic Current RAFOS float observations, *J. Geophys. Res.*, *106*, 13,817–13,836, 2001.

A. Griffa, A. J. Mariano, A. Molcard, and T. M. Özgökmen, Rosenstiel School of Marine and Atmospheric Sciences (RSMAS)/MPO, University of Miami, Miami, FL, USA. (amolcard@rsmas.miami.edu)

L. I. Piterbarg, Center for Applied Mathematical Sciences, University of Southern California, Los Angeles, CA, USA.